

Theory of atomic chemisorption on simple metals

N. D. Lang and A. R. Williams

IBM Thomas J. Watson Research Center, Yorktown Heights, New York 10598

(Received 20 December 1977)

We use the atom-jellium model of chemisorption to study the properties of an atom bonded to the surface of a simple metal. Beyond the jellium simulation of the metal substrate and the Kohn-Sham local-density description of exchange and correlation, we make no significant approximations: our solutions are parameter free, wave mechanical, and fully self-consistent. We solve this model for a set of adatoms exhibiting a variety of chemical behaviors. Properties studied include the electron-density distribution, the state density, the dipole moment, and the heat of adsorption. We discuss also the reintroduction of the discrete lattice structure of the substrate using perturbation theory.

I. INTRODUCTION AND MODEL

The chemical bond formed between an atom and a metal surface has been the subject of much recent theoretical attention. Brief critical reviews of the various approaches employed have been given by a number of authors.¹⁻⁵ In the present treatment, we employ the density-functional method of Kohn, Hohenberg, and Sham⁶⁻⁸ because of its basic structural simplicity and its success in a wide range of problems in the study of surfaces,^{9,10} atoms and molecules,¹¹ and solids.¹² The analyses of chemisorption which employ this method can be divided into those which use a model for the substrate that has a continuous spectrum of eigenstates (in particular a semi-infinite substrate)¹³⁻²⁰ and those which use a model that has a discrete spectrum (a small cluster of substrate atoms).²¹ A discussion of the adequacy of the cluster simulation, as well as a prescription for combining features of both types of substrate simulation (cluster embedding) has been given by Grimley.^{1,22}

The present study considers a single atom chemisorbed on a semi-infinite metallic substrate.²³ The substrate is represented using the uniform-background (jellium) model, which has given good results for the ground-state properties of the surfaces of simple (*s-p* bonded) metals.^{9,24-26} This treatment is not intended to apply to chemisorption on transition metals, which have a more complex density-of-states structure and a greater ability to exhibit directional bonding. An important reason for the study (both theoretical and experimental) of chemisorption on simple metals, in addition to its intrinsic interest, is to assist in understanding which of the aspects of chemisorption on more complex metallic substrates result from this greater complexity, and which result only from the fact that the substrate has a continuous energy spectrum.

The aim of the present analysis is to obtain, using the Kohn-Sham local-density description of exchange and correlation,⁷ self-consistent numerical solutions for the properties of a simple model without the use of any other significant approximation. We confine our consideration to chemisorption systems in which neither important spin fluctuations nor permanent moments are expected to be present,²⁷ and we thus use the spin-unpolarized form of the method of Kohn and Sham.²⁸ The only input to our calculation is the adatom nuclear charge Z and the positive background density of the substrate (specified by r_s).²⁹ We introduce no adjustable parameters, no assumed variational forms for the wave functions, and no assumption of spherical symmetry near the nucleus. All of the adatom core states are computed self-consistently, including polarization effects. The care taken in the treatment of the model permits us to bring out its full physical and chemical content, and allows us to understand the final results (quantities accessible experimentally) by examining the internal structure and intermediate results in the calculation.

Other self-consistent studies in the literature of the chemisorption of a single atom on a simple metal, which we can compare with the present treatment, are as follows: One group of studies is represented by the work of Smith, Ying, and Kohn,²³ which treats the same model, for the case of hydrogen chemisorption, but employs two significant approximations not used in the present work: an extended Thomas-Fermi treatment of the kinetic energy, and the assumption that the substrate can be taken to respond linearly to the adatom nucleus (proton). Although the equilibrium distance obtained is similar to that found here, the approximations do not appear to permit an adequate description of the dipole moment, electron density near the nucleus or heat of atomic adsorption (see Ref. 14 for details). The work of

Gunnarsson, Hjelmberg, and Lundqvist,¹⁸ again only for hydrogen chemisorption, uses the same model and approach as the present work, but employs a different analytical framework. The results given for the equilibrium distance, density of states and heat of adsorption are similar to those described here and in Ref. 14. The work of Harris and Painter²¹ for oxygen chemisorption on aluminum exemplifies the cluster approach. For metal-adsorbate separations other than those corresponding to incorporation of the oxygen by the Al lattice, the results for the energy spectrum are very similar to those found in the present work, which in turn resemble the results of measurements for the Al(111) surface (see Sec. III below). On loosely packed faces of Al, however, the oxygen appears to be incorporated into the surface, and the cluster calculations of Messmer and Salahub²¹ indicate that in this case, local molecular bonding effects not present in the atom-jellium model can play an important role.

II. METHOD OF SOLUTION

We provide here a description of the theory used to obtain the results discussed in Sec. III. We begin with an outline of the logical structure of the theory; we do this for two reasons: first, for readers not interested in the theoretical details, the outline offers a description of the theory sufficient to understand the results, and second, it provides a guide to the more detailed discussion which follows.

The entire analysis is based, as noted above, on the density-functional theory of many-electron systems, which requires the solution of effective one-electron, Schrödinger-like equations. The present analysis casts these single-particle equations into scattering-theoretic (or Lippmann-Schwinger) form

$$\Psi^{MA}(\vec{r}) = \Psi^M(\vec{r}) + \int d^3r' G^M(\vec{r}, \vec{r}') \delta v_{\text{eff}}(\vec{r}') \times \Psi^{MA}(\vec{r}'). \quad (2.1)$$

The superscripts M and MA refer, respectively, to the bare metal and the combined metal-adsorbate system. Equation (2.1) embodies the notion that electrons in stationary states of the semi-infinite metal $[\Psi^M(\vec{r})]$ impinge on and are scattered elastically by the potential $\delta v_{\text{eff}}(\vec{r})$, which describes the difference between the perturbed (combined metal-adsorbate) system and the bare metal.

The Schrödinger differential equation corresponding to Eq. (2.1) can be solved exactly by direct numerical integration outward from the adsorbate nucleus. Solutions $\Psi_i(\vec{r})$ obtained in this way are characterized by their angular behavior near the

nucleus and do not in general satisfy the boundary conditions embodied in the Lippmann-Schwinger equation; the desired solution is, however, a linear combination of these fundamental solutions,

$$\Psi^{MA}(\vec{r}) = \sum_i C_i \Psi_i(\vec{r}), \quad (2.2)$$

where the coefficients C_i are obtained by substituting Eq. (2.2) into Eq. (2.1).

The remainder of this section is devoted to the details of the procedure just described; these can be grouped as follows (in the order in which they appear in the text): (i) Specification of the differential equations and the effective one-electron potential provided by our use of the local-density approximation within the density-functional framework. (ii) Replacement of the volume integration in the Lippmann-Schwinger equation by the equivalent surface integral, in order to reduce the number of coordinate values \vec{r}' at which the bare-metal Green's function $G^M(\vec{r}, \vec{r}')$ must be evaluated. (iii) Further manipulations of Eq. (2.1) aimed at improving the numerical accuracy of the calculations by, for example, focusing directly on the difference $\Psi^{MA}(\vec{r}) - \Psi^M(\vec{r})$. (iv) Specification and construction of the bare-metal functions $\Psi^M(\vec{r})$. (v) Calculation of the fundamental solutions $\Psi_i(\vec{r})$. (These are constructed in a spherical coordinate system centered on the nucleus, and are represented as radially varying combinations of spherical harmonics.) (vi) Specification and construction of $G^M(\vec{r}, \vec{r}')$. (vii) Discussion of the particular way in which we have treated the \vec{r} dependence of the equation obtained by substituting Eq. (2.2) into Eq. (2.1), in order to obtain independent equations specifying the coefficients C_i while minimizing the number of coordinate values \vec{r} at which $G^M(\vec{r}, \vec{r}')$ must be evaluated.

The formalism of Kohn and Sham, as indicated above, reduces the many-body problem for the ground-state density distribution $n(\vec{r})$ of an inhomogeneous system of N electrons in a static external potential $v(\vec{r})$ (due here to the adsorbate nucleus and the positive background) to the self-consistent solution of the equations (we use Rydberg units, with $|e| = 2m = \hbar = 1$)

$$(-\nabla^2 + v_{\text{eff}}[n; \vec{r}])\Psi_i(\vec{r}) = E_i \Psi_i(\vec{r}) \quad (2.3a)$$

$$n(\vec{r}) = \sum_i |\Psi_i(\vec{r})|^2 n_i, \quad (2.3b)$$

where n_i indicates the occupation of the i th (orthonormal) orbital. In the metal-adsorbate system, $n_i = 1$ if E_i is less than the Fermi energy (we label the two members of a Kramers-degenerate pair by different i values), and $n_i = 0$ otherwise. The

potential in Eq. (2.3a) is given by

$$v_{\text{eff}}[n; \vec{r}] = v(\vec{r}) + 2 \int \frac{n(\vec{r}')}{|\vec{r} - \vec{r}'|} d^3r' + v_{xc}[n; \vec{r}], \quad (2.4)$$

where $v_{xc}[n; \vec{r}]$ is an exchange-correlation potential, the "local-density" approximation⁷ to which is

$$\begin{aligned} v_{xc}(n(\vec{r})) &= \left. \frac{dn\epsilon_{xc}(n)}{dn} \right|_{n=n(\vec{r})} \\ &= -2 \left(\frac{3}{\pi} \right)^{1/3} n(\vec{r})^{1/3} + \left. \frac{dn\epsilon_c(n)}{dn} \right|_{n=n(\vec{r})}. \end{aligned} \quad (2.5)$$

[The factors of 2 appearing in Eqs. (2.4) and (2.5) arise from the use of Rydberg energy units.] Here $\epsilon_{xc}(n)$ is the exchange-correlation energy per particle of a uniform electron gas of density n and $\epsilon_c(n)$ is the correlation part. (The expression for ϵ_c used in the present study is that given by Hedin and Lundqvist.³⁰) The total energy of the system in this case is

$$\begin{aligned} E_{\text{tot}} &= \sum_i E_i n_i - \int d^3r v_{\text{eff}}[n; \vec{r}] n(\vec{r}) \\ &+ \int d^3r \epsilon_{xc}(n(\vec{r})) n(\vec{r}) + E_{\text{es}}, \end{aligned} \quad (2.6)$$

where E_{es} is the total electrostatic energy of the system.

We wish to solve Eqs. (2.3) self-consistently for the atom-jellium model introduced above, consisting of a semi-infinite uniform positive background, a nucleus of charge Z , and the gas of interacting electrons. Now the metal screens out the effects of the adatom on the charge density and potential, except in the adatom's vicinity. (The disturbance in the individual single-particle wave functions is not short-ranged, however.) It is this locality of the disturbance in the potential that is conveniently exploited, for the continuum states (i.e., states above the bottom of the metal band), by using the Lippmann-Schwinger integral equation corresponding to Eq. (2.3a).

Let us call the electron number density in the metal-adatom system $n^{MA}(\vec{r})$; and let us denote the corresponding density for the bare metal by $n^M(\vec{r})$. The eigenfunctions Ψ^{MA} and Ψ^M will be specified by an energy eigenvalue E and other labels, but we omit these for now. Thus, we write the differential equations satisfied by these eigenfunctions

$$(\nabla^2 + E - v_{\text{eff}}[n^M; \vec{r}])\Psi^M(\vec{r}) = 0 \quad (2.7a)$$

$$(\nabla^2 + E - v_{\text{eff}}[n^{MA}; \vec{r}])\Psi^{MA}(\vec{r}) = 0. \quad (2.7b)$$

The Lippmann-Schwinger equation equivalent to

Eq. (2.7b) (and its boundary conditions) for the continuum states is given above as Eq. (2.1), where $G^M(\vec{r}, \vec{r}')$ (the outgoing-wave Green's function for the bare metal, from which we omit the label E for now) satisfies the equation

$$(\nabla^2 + E - v_{\text{eff}}[n^M; \vec{r}])G^M(\vec{r}, \vec{r}') = \delta(\vec{r} - \vec{r}'), \quad (2.8)$$

and where

$$\delta v_{\text{eff}}(\vec{r}) = v_{\text{eff}}[n^{MA}; \vec{r}] - v_{\text{eff}}[n^M; \vec{r}]. \quad (2.9)$$

Equation (2.1), together with Green's theorem and the fact that

$$\delta v_{\text{eff}}(\vec{r})\Psi^{MA}(\vec{r}) = (\nabla^2 + E - v_{\text{eff}}[n^M; \vec{r}])\Psi^{MA}(\vec{r}) \quad (2.10),$$

implies

$$\begin{aligned} \oint_S d\vec{S}' \cdot [\Psi^{MA}(\vec{r}') \vec{\nabla}_{r'} G^M(\vec{r}, \vec{r}') \\ - G^M(\vec{r}, \vec{r}') \vec{\nabla}_{r'} \Psi^{MA}(\vec{r}')] = \Psi^M(\vec{r}) \end{aligned} \quad (2.11)$$

for \vec{r} within the (closed) surface S . (S can be any surface outside of which δv_{eff} is negligible.) We recognize the above surface integral as the operator which projects out of a scattering solution the unscattered wave. For computational accuracy, it is better to work with an equation for just the scattered wave $\delta\Psi \equiv \Psi^{MA} - \Psi^M$, and so we proceed as follows: Since Eq. (2.11) is true for any δv_{eff} , in particular $\delta v_{\text{eff}} = 0$, we can obtain another equation by replacing Ψ^{MA} by Ψ^M on the left-hand side. Subtracting this from Eq. (2.11) then yields an equation satisfied by $\delta\Psi$:

$$\begin{aligned} \oint_S d\vec{S}' \cdot [\delta\Psi(\vec{r}') \vec{\nabla}_{r'} G^M(\vec{r}, \vec{r}') \\ - G^M(\vec{r}, \vec{r}') \vec{\nabla}_{r'} \delta\Psi(\vec{r}')] = 0, \end{aligned} \quad (2.12)$$

where \vec{r} is within S .

In addition to the two-dimensional translational symmetry of the bare surface which makes the computation of $G^M(\vec{r}, \vec{r}')$ tractable, the most important symmetry in the problem is the cylindrical symmetry of the charge density and potential in the atom-jellium system. In accordance with this, we introduce cylindrical coordinates ρ, ϕ, z , with the origin taken at the position of the adatom nucleus and the z axis along the outward surface normal (see Fig. 1). The eigenfunctions of Eq. (2.7a) for the bare metal can then be written using this coordinate system

$$\Psi_{E\kappa}^M(\vec{r}) = e^{im\phi} J_m(\kappa\rho) u_{E\kappa}^M(z), \quad (2.13)$$

whose normalization is given by

$$\begin{aligned} \int d^3r [\Psi_{E\kappa}^M(\vec{r})]^* \Psi_{E'\kappa'}^M(\vec{r}) \\ = \delta(E - E') \delta(\kappa - \kappa') \delta_{mm'}. \end{aligned} \quad (2.14)$$

The functions $u_{E\kappa}^M(z)$ (with E below the vacuum level) decay exponentially in the vacuum ($z \rightarrow \infty$), and are oscillatory deep in the metal ($z \rightarrow -\infty$):

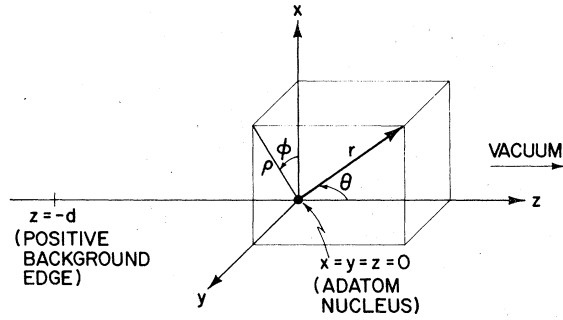


FIG. 1. Cylindrical and spherical coordinate systems used here have a common origin at the adatom nucleus, which is a distance d to the right of the positive-background edge. The background fills the $z < -d$ half space.

$$u_{E\kappa}^M(z) \rightarrow \pi^{-1} \kappa^{1/2} (2k)^{-1/2} \sin[kz - \gamma(k)], \quad (2.15)$$

where

$$k = (E - \kappa^2 - E_0)^{1/2}, \quad (2.16)$$

with $E_0 \equiv v_{\text{eff}}(-\infty)$ the value of v_{eff} deep in the metal (i.e., the bottom of the metal band). The quantum numbers E , m , and κ reflect the quantities conserved by the symmetry of the bare model surface: energy and the two components (angular and radial) of transverse momentum.

The continuum eigenfunctions $\Psi^{MA}(\vec{r})$ for the chemisorbed system, which are solutions to the Lippmann-Schwinger equation (2.1) will, via this equation, have the same labeling (E, m, κ) as the Ψ^M , even though of course κ no longer refers to a conserved quantity. These solutions will also have the same normalization as the Ψ^M [given by Eq. (2.14)],³¹ a fact which facilitates the calculation of the electron-density distribution and the state density.

Within the surface S , we write the eigenfunctions $\Psi_{E m \kappa}^{MA}$ (and $\Psi_{E m \kappa}^M$ as well) in terms of solutions $\Psi_{E m l}^{MA}$ ($\Psi_{E m l}^M$) of the same differential equation (2.7b) [(2.7a)] with the same E and m , but which are labeled by their behavior at the origin (the position of the adatom nucleus):

$$\lim_{r \rightarrow 0} r^{-l} \int d\Omega Y_{l m}^*(\Omega) \Psi_{E m l}^{MA}(\vec{r}) = \delta_{ll'}, \quad (2.17)$$

where $M(A)$ means either M or MA . (The functions $\Psi_{E m l}^{MA}$ are the fundamental solutions referred to as Ψ_l in the outline above.) In describing these functions we use the spherical coordinate system r, θ, ϕ shown in Fig. 1. $\Psi_{E m l}^{MA}$ and $\Psi_{E m l}^M$ can be found by direct numerical integration of the differential equation out from the origin (see Appendix A) using the method of Williams and Morgan.³² We write

$$\Psi_{E m \kappa}^{M(A)}(\vec{r}) = \sum_{l'=|m|}^{\infty} \alpha_{E m \kappa l'}^{M(A)} \Psi_{E m l'}^{M(A)}(\vec{r}). \quad (2.18)$$

With $\delta\alpha = \alpha^{MA} - \alpha^M$ and $\delta\Psi = \Psi^{MA} - \Psi^M$, we can write (omitting the E, m subscripts common to all quantities),

$$\delta\Psi_{\kappa}(\vec{r}) = \sum_{l'=|m|}^{\infty} [\alpha_{\kappa l'}^M \delta\Psi_{l'}(\vec{r}) + \delta\alpha_{\kappa l'} \Psi_{l'}^{MA}(\vec{r})]. \quad (2.19)$$

We can use Eq. (2.18) to determine the coefficients $\alpha_{\kappa l}^M$ that appear here, in view of the facts that $\Psi_{l'}^M$ (we continue to omit E, m) is known from the numerical integration mentioned above and that Ψ_{κ}^M can be obtained from the self-consistent calculations for the bare surface described by Lang and Kohn.²⁵ This leaves only $\delta\alpha_{\kappa l}$ to be determined in order to specify $\delta\Psi_{\kappa}$, since $\Psi_{l'}^{MA}$ and $\delta\Psi_{l'} = \Psi_{l'}^{MA} - \Psi_{l'}^M$ are known by numerical integration. In actually using Eq. (2.19) for $\delta\Psi_{\kappa}$, we will make the completely controllable approximation of replacing the upper limit of the l sum by an l_{max} ($l_{\text{max}}=6$ was found to be entirely sufficient in the present work). We are able in this way to find the continuum eigenfunctions $\Psi_{\kappa}^{MA} (= \Psi_{\kappa}^M + \delta\Psi_{\kappa})$.³³

We now discuss the determination of the coefficients $\delta\alpha$ in Eq. (2.19). Substitution of Eq. (2.19) (with l_{max} as the upper limit on the l sum) into Eq. (2.12) yields an equation of the form (omitting E, m, κ)

$$\sum_{l'=|m|}^{l_{\text{max}}} A_{l'}(\vec{r}) \delta\alpha_{l'} = B(\vec{r}). \quad (2.20)$$

Equations sufficient in number to determine the coefficients $\delta\alpha_l$ could be obtained by taking \vec{r} to have N_l ($\equiv l_{\text{max}} + 1 - |m|$) arbitrary values within the volume bounded by the surface S . A more convenient treatment of this \vec{r} dependence, however, is suggested by the structure of $G^M(\vec{r}, \vec{r}')$, which enters both $A_l(\vec{r})$ and $B(\vec{r})$.

By virtue of the completeness of the sets of functions $J_m(\kappa\rho)$ and $e^{im\phi}$, we see from Eq. (2.8) that we can write

$$G_E^M(\vec{r}, \vec{r}') = \frac{1}{2\pi} \sum_{m=-\infty}^{\infty} e^{im(\phi-\phi')} \times \int_0^{\infty} \kappa d\kappa J_m(\kappa\rho) \times J_m(\kappa\rho') \bar{u}_{E\kappa}^M(z_<) u_{E\kappa}^M(z_>) W_{E\kappa}^{-1}, \quad (2.21)$$

where $z_< (z_>)$ is the lesser (greater) of z and z' . The functions u^M and \bar{u}^M satisfy the equations

$$\left(\frac{d^2}{dz^2} + E - \kappa^2 - v_{\text{eff}}[z^M; z] \right) \times \left\{ \begin{array}{l} u_{E\kappa}^M(z) \\ \bar{u}_{E\kappa}^M(z) \end{array} \right\} = 0. \quad (2.22)$$

As mentioned earlier, the regular solution $u^M \rightarrow 0$ as $z \rightarrow -\infty$.³⁴ In the limit $z \rightarrow -\infty$, u^M has the sine wave form of Eq. (2.15) when $k^2 > 0$ [see (2.16)] and increases exponentially when $k^2 < 0$. On the other hand, the appropriate irregular solution \bar{u}^M increases exponentially as $z \rightarrow \infty$ and is proportional to $\exp(-ikz)$ for $z \rightarrow \infty$, with $\arg k = 0$ for $k^2 > 0$ and $\arg k = \frac{1}{2}\pi$ for $k^2 < 0$. The Wronskian $W_{E\kappa}$ that appears in Eq. (2.21), defined by

$$W = \bar{u}^M(z) \frac{du^M(z)}{dz} - u^M(z) \frac{d\bar{u}^M(z)}{dz} \quad (2.23)$$

(omitting the E and κ subscripts common to all quantities), is independent of z .

The structure of the bare-metal Green's function

$$\begin{aligned} & \sum_{l'=|m|}^{l_{\max}} \delta\alpha_{\kappa l'} \int_{-1}^1 d \cos \theta \left(G_l^M(r, \theta) \frac{\partial}{\partial r} \psi_l^{MA}(r, \theta) - \psi_l^{MA}(r, \theta) \frac{\partial}{\partial r} G_l^M(r, \theta) \right)_{r=R} \\ &= - \sum_{l'=|m|}^{l_{\max}} \alpha_{\kappa l'} \int_{-1}^1 d \cos \theta \left(G_l^M(r, \theta) \frac{\partial}{\partial r} \delta\psi_{l'}(r, \theta) - \delta\psi_{l'}(r, \theta) \frac{\partial}{\partial r} G_l^M(r, \theta) \right)_{r=R} \end{aligned} \quad (2.24)$$

where

$$e^{im\phi} \psi_{E_{ml}}^{M(A)}(r, \theta) = \Psi_{E_{ml}}^{M(A)}(\vec{r}) \quad (2.25)$$

and

$$\begin{aligned} G_{E_{ml}}^M(r, \theta) &= \lim_{r' \rightarrow 0} r'^{-l} \int_{-1}^1 d \cos \theta' \int_0^{2\pi} d(\phi - \phi') Y_{lm}^*(\Omega') \\ &\quad \times e^{im\phi} G_E^M(\vec{r}, \vec{r}'). \end{aligned} \quad (2.26)$$

We use here the periodicity of $G_E^M(\vec{r}, \vec{r}')$ in $(\phi - \phi')$ and the symmetry in \vec{r} and \vec{r}' that is evident from

just described is most conveniently exploited in the following way. Multiply both sides of Eq. (2.20) by $r^{-l} Y_{lm}^*(\Omega)$ (with l taking values from $|m|$ to l_{\max}), integrate over solid angle Ω , and then let $r \rightarrow 0$. (The fact that the Green's function to which this limit procedure is applied is given in cylindrical rather than spherical coordinates, and that furthermore its z dependence is known only numerically, means that special care is required in taking the limit—see Appendix B.) For convenience, we take the surface S to be a sphere of radius R (with R large enough that $\delta v_{\text{eff}} \approx 0$ outside the sphere); the equation for $\delta\alpha$ (2.20) then becomes (omitting the E, m subscripts common to all quantities, and with \vec{r}' and \vec{r} interchanged)

Eq. (2.21). (The detailed form of $G_{E_{ml}}^M$ is given in Appendix B.) Equation (2.24) is fundamentally the spherical harmonic decomposition of Eq. (2.20). It is a system of linear equations (in l_{\max} and l') which determines the coefficients $\delta\alpha_{E_{m\kappa} l}$; using these coefficients as described above, we obtain the continuum states in the metal-adatom system $\Psi_{E_{m\kappa}}^{MA}$. The calculation of the discrete states $\Psi_{E_c m}^{MA}$ (with E_c the energy eigenvalue,³⁵ which will in general depend on m) is described in Appendix A.

Given these functions we will calculate (within the sphere of radius R)³⁶

$$\delta n(\vec{r}, E) = 2 \sum_{m=-\infty}^{\infty} \left(\Theta(E - E_0) \int_0^{(E - E_0)^{1/2}} d\kappa [|\Psi_{E_{m\kappa}}^{MA}(\vec{r})|^2 - |\Psi_{E_{m\kappa}}^M(\vec{r})|^2] + \sum_c |\Psi_{E_c m}^{MA}(\vec{r})|^2 \delta(E - E_c) \right). \quad (2.27)$$

The factor of 2 is for spin degeneracy (recall that we use a spin-unpolarized formalism). Note that $\delta n(\vec{r}, E)$ is independent of ϕ (i.e., is cylindrically symmetric). The difference in electron density between the metal-adatom system and the bare metal is

$$\delta n(\vec{r}) = n^{MA}(\vec{r}) - n^M(\vec{r}) = \int_{-\infty}^{E_F} dE \delta n(\vec{r}, E), \quad (2.28)$$

where $E_F = E_0 + k_F^2$ [$k_F \equiv (9\pi/4)^{1/3}/r_s$]. The electron density in the metal-adatom system (n^{MA}) is evaluated as $n^M(\vec{r}) + \delta n(\vec{r})$ with n^M calculated di-

rectly as described in Ref. 25. This is then used to reevaluate v_{eff} using Eq. (2.4); and a self-consistent density distribution for the metal-adatom system is obtained by iteration.³⁷ (The way in which charge disturbances outside the sphere of radius R are taken into account is described in Appendix C.³⁸)

It is convenient also to define a difference of eigenstate density as

$$\delta n(\mathbf{E}) = \int d^3r \delta n(\vec{r}, \mathbf{E}). \quad (2.29)$$

The adatom dipole moment μ is defined as

$$\mu = - \int d^3r z \delta n(\vec{r}) \quad (2.30)$$

(recall that $z \rightarrow \infty$ is in the vacuum). Since $z=0$ is at the nucleus, the nuclear charge does not appear in this formula. The atomic binding energy ΔE_a is the difference in total energy between the metal plus the separated atom³⁹ and the metal with the atom chemisorbed on its surface. The energies are calculated using Eq. (2.6); note that the difference in the first term in this equation ($\sum E_i n_i$) between the metal-adatom system and the bare metal can be evaluated simply as

$$\int_{-\infty}^{E_F} dE \delta n(E) E.$$

III. SELECTED RESULTS AND THEIR INTERPRETATION

We present calculations for a representative set of adatoms (H, Li, O, Na, Si, Cl) which exhibit a variety of chemical behavior, chemisorbed on a high-density metallic substrate [$r_s=2$, which simulates such simple (i.e., s - p bonded) metals as Al ($r_s=2.07$), Zn ($r_s=2.30$), and Mg ($r_s=2.65$)]. Some results are included for $r_s=4$ (\sim Na density) in order to illustrate the dependence on this parameter. The reader should recall that r_s and the adatom nuclear charge Z are the only parameters in the atom-jellium model. The equilibrium distance d_{eq} between the adatom nucleus and the positive background edge is obtained by minimizing the calculated total energy.

Table I gives d_{eq} for these six atoms, along with the corresponding value of the atomic binding energy ΔE_a . We note in this connection that the positive-background edge from which d is measured is to be considered to be half an interplanar spacing in front of the outermost lattice plane of the substrate being simulated, by construction of the jellium model.⁹ (We defer to the end of this section a discussion of the relationship between these results and experimental measurements.)

TABLE I. Equilibrium distance d (adatom nucleus to positive-background edge) and atomic binding energy ΔE_a for adsorption on a high-density ($r_s=2$) substrate. The changes that occur in these quantities when the discrete lattice is reintroduced using perturbation theory are discussed in Appendix D (see also Refs. 15, 16, 18, 19, and 46). (Note that the outermost substrate lattice plane lies half an interplanar spacing behind the background edge.)

Adatom	d_{eq} (bohrs)	ΔE_a (eV)
H	1.1	1.5
Li	2.5	1.3
O	1.1	5.4
Na	3.1	0.9
Si	2.3	3.0
Cl	2.6	3.6

The difference of eigenstate density $\delta n(E)$ defined in Eq. (2.29) is shown in Fig. 2 for the atoms Li, Si, and Cl. The location of the resonances in this figure relative to the Fermi level (E_F) determines the degree of occupation; the three cases shown exhibit the range of possible behavior. The $2s$ resonance of Li lies primarily above E_F and the $3p$ resonance of Cl lies below, providing clear examples of positive and negative ionic chemisorption. The direction of charge transfer is consistent with the magnitudes of the electronegativities of Li, Cl, and a high-density metallic substrate (such as Al). [Approximate integration of the atomic-difference density shown in Fig. 3 (discussed below) suggests that the Cl- $3p$ resonance, despite its energy position below E_F , contains less than six electrons. This is apparently a reflection of an effect discussed by Pendry⁴⁰ in which a portion of the spectral weight of such resonances is spread over a wide energy region.

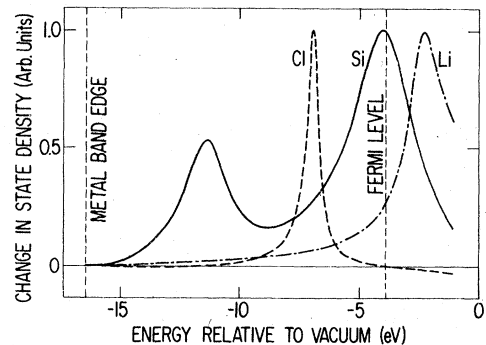


FIG. 2. Change in state density $\delta n(E)$ due to chemisorption. Curves correspond to metal-adatom distance d which minimizes the total energy (Table I). High-density ($r_s=2$) substrate. Note that the lower Si resonance corresponds to the $3s$ level of the atom; for Cl this is a discrete state below the band edge.

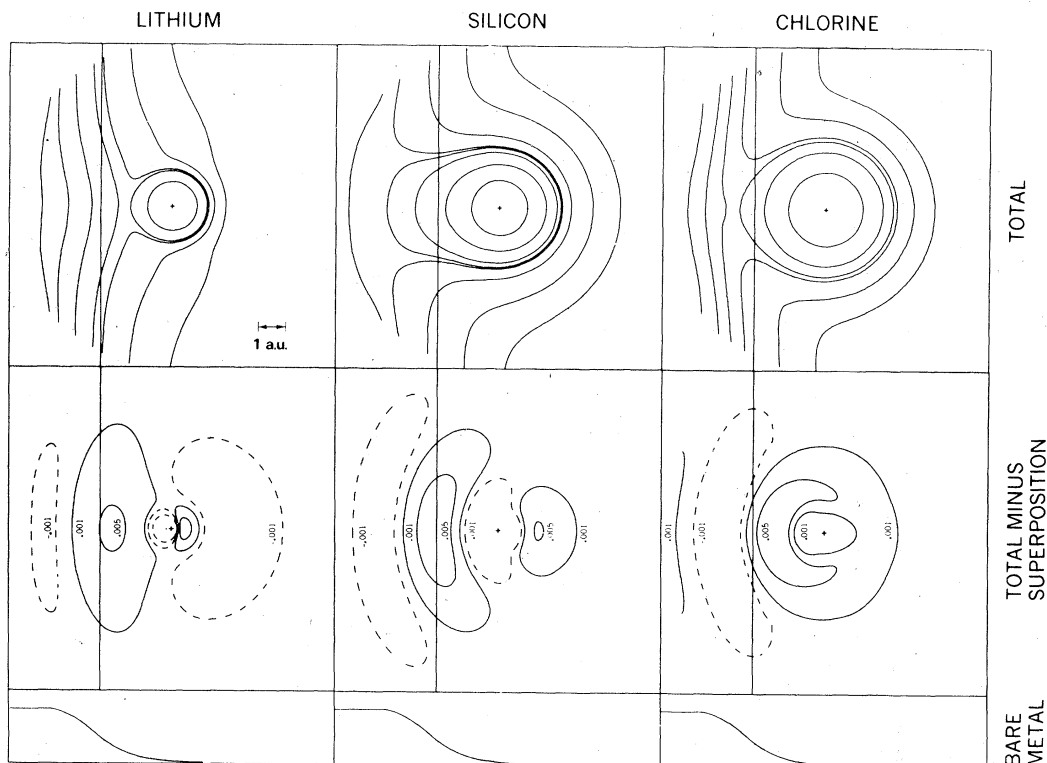


FIG. 3. Electron-density contours for chemisorption on a high-density ($r_s=2$) substrate. Metal-adatom distances shown minimize the total energy. Upper row: Contours of constant electron density in (any) plane normal to the metal surface containing the adatom nucleus (indicated by +). Metal is to the left-hand side; solid vertical line indicates positive-background edge. For computational convenience, contours are not shown outside the inscribed circle of each square. Contour values are selected to be visually informative. Center row: Total electron density minus the superposition of atomic and bare-metal electron densities (electrons/bohr³). The polarization of the core region, shown for Li, has been deleted for Si and Cl because of its complexity. Bottom row: Bare-metal electron-density profile (shown to establish physical distance scale). (For reference, the bulk metal density is 0.03 electrons/bohr³.)

Another example of this effect is the fact that the d bands of metallic Cu contain only 9.6 electrons.^{41]} The energetic cost of completely filling or emptying the Si- $3p$ resonance results in its self-consistent partial occupation; this leads in turn to a clearly discernible covalent bond charge (see below).

The spatial manifestation of the three types of behavior exhibited in Fig. 2 is given by the charge density contours of Fig. 3. An important reason for considering such density maps is that they provide a spatially detailed picture of bonding which is independent of the analytical approach employed. Further, the existence of comprehensive analyses of electron densities in related molecular systems⁴² makes it possible to compare the chemical trends in these extensively studied systems with those in chemisorption. (This comparison is also relevant to the adequacy of simulating surface complexes with small clusters.)

Contours of constant density are shown in Fig. 3

for both the total electron density in the metal-adatom system (upper row) and the total minus the superposition of bare-metal and free-atom³⁹ electron densities (center row). The outermost closed total-density contours surrounding the Li and Cl nuclei are more nearly circular than those for Si, which show a more prominent projection of charge into the bond region. The metal contours in these total-density maps deflect toward the Li and away from the Cl, indicating the ionic attraction (Li) and repulsion (Cl). The relative rapidity with which the contours regain their bare-metal form outside the immediate vicinity of the adatom is an illustration of the effectiveness of metallic screening.

The difference contours in Fig. 3 show clearly the displacements of electronic charge which accompany bonding. In Li, we see that charge is transferred from the vacuum side of the adatom toward the metal. The kidney-shaped depletion contour on the vacuum side, and even the reverse

dipole contours in the core region, are very similar to those found by Bader and co-workers⁴² in the LiH and LiF molecules. The nearly empty Li resonance of Fig. 2 suggests that the transferred electrons are to be thought of as residing in "metal" states. (It should be recalled that our calculations do not define distinct atom and metal states.) Note also that for Li, as well as for the other two cases, the sequence of contours continues into the metal in the form of Friedel oscillations induced by the perturbing atom. The difference contours for Si show a depletion of charge near the nucleus and accumulations on both the bond and vacuum sides. The same general behavior is found in all of the diatomic molecules studied in Ref. 42 which exhibit *p*-orbital covalent bonding. The difference contours for Cl provide a picture of a polarized negative ion similar to that found for H and F in the molecular calculations just mentioned.

The connection between the covalent bond charge seen for Si in the contour maps and the partial occupation of the valence resonance is exhibited in Fig. 4. Contour plots of $\delta n(\vec{r}, E)$ are shown for four values of E : one value each from the low-energy and high-energy parts of both valence resonances. We identify these two valence resonances as arising from the 3*s* and 3*p* atomic levels. There are two basic interactions of interest in this case: the interaction between each atomic level and the metal, and the intra-atomic mixing of the two levels (3*s* and 3*p_x*) due to the asymmetry of the surface potential. The interaction with the metal broadens each level into a resonance, whose lower part adds charge to the bond region ("bonding") and whose upper part subtracts charge from this region ("antibonding"). The interaction between the levels provides an overall polarization to the charge distributions associated with each level—into the bond region for the "3*s*" charge distribution and into the vacuum for the "3*p*" charge. Note that the two effects tend to work in opposite directions in the cases labeled "antibonding *s*" and "bonding *p*" in Fig. 4, particularly in the latter case, as seen in the contour plot. The fact that the upper part of the 3*p* resonance is unoccupied means that the negative contribution it would make to the charge density in the bond region is not present, and that there is a net accumulation of bond charge from the states that are occupied. [If, in calculating $\delta n(\vec{r})$, we fill the 3*p* resonance to just below the vacuum level, without recalculating the states, and add this $\delta n(\vec{r})$ to the bare-metal density, then the corresponding total-density contour map no longer resembles that of Si in the upper row of Fig. 3, but instead resembles that of Cl.]

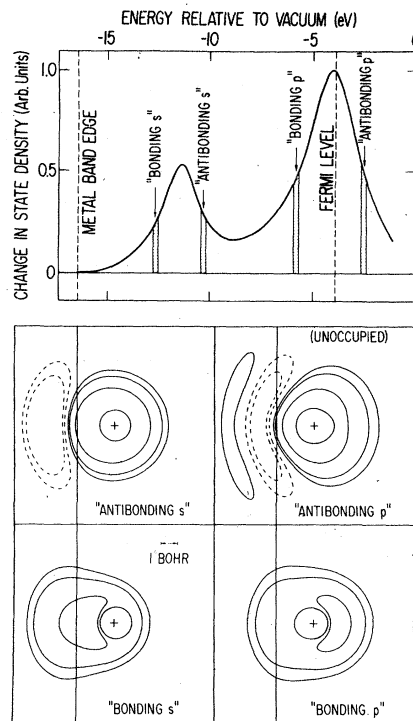


FIG. 4. Upper part of figure reproduces the state density curve from Fig. 2 for Si chemisorbed at its equilibrium distance on a high-density ($r_s=2$) substrate. The two peaks correspond to the 3*s* and 3*p* atomic states. The lower part of the figure shows the density contours [contours of $\delta n(\vec{r}, E)$] associated with the four shaded regions in the state density curve. (See caption of Fig. 3 for details of such contour maps.) Solid lines correspond to positive contour values, dashed lines to negative values. The same set of contour values was used for all four cases. The crescent-shaped contours in the two "bonding" maps correspond to maxima in the density. (Contours near the nucleus have been deleted for clarity.)

While our calculations predict an equilibrium metal-atom separation, the results of calculations performed for other separations provide theoretical insight into the distance dependence of the metal-atom interaction; of particular interest are the variations of the state-density difference $\delta n(E)$ and the dipole moment μ .

In Fig. 5, $\delta n(E)$ is shown for a chemisorbed hydrogen atom at three different distances. At the largest distance, the metal-atom interaction is not strong, and the resonance that is present below the Fermi level is relatively narrow. When the atom is moved closer, this interaction increases, and the resonance widens considerably. It also moves further below the Fermi level, showing a tendency to follow the bare-metal surface potential. When the atom is moved still

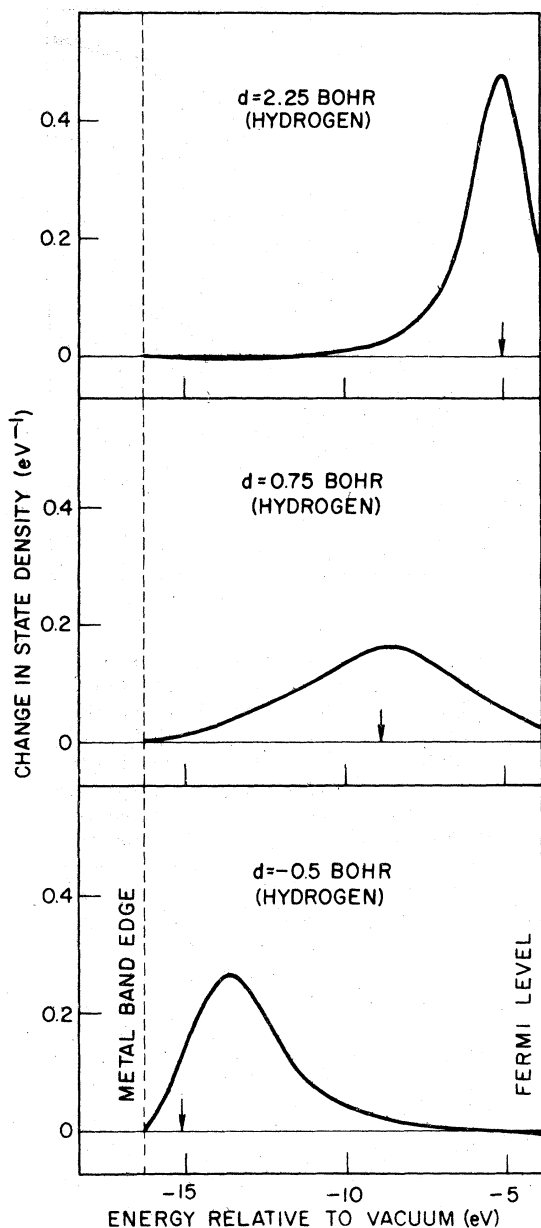


FIG. 5. State density change $\delta n(E)$ due to chemisorption of H on a high-density ($r_s = 2$) substrate. Curves are shown for three different metal-atom distances d . Arrow gives value of bare-metal potential $v_{\text{eff}}[n^M; z]$ at adatom nucleus; zero of potential is set so that arrow falls under peak of resonance for largest distance. This shows the way in which the resonance position roughly follows the surface potential—see text. (If the arrows had been drawn for v_{es} instead of v_{eff} , the arrow in the bottom panel would have been to the right of the peak, indicating as expected from the discussion in the text, that the actual calculated behavior of the resonance is intermediate between the two potentials.)

closer, the broadening due to increasing metal-adatom interaction is overtaken by narrowing due to the decreasing density of metal states seen by the resonance as it moves down toward the bottom of the metal band, and the resonance narrows again.^{43, 44}

We find quite generally that the energy positions of adatom valence resonances tend to follow the bare-metal surface potential as the atom is moved into the surface. This is true as well for the discrete states of the adatom that belong to the same principal quantum-number shell as the valence resonance, such as the 3s state in Cl. Let us consider briefly why this should be true. It is simplest to think of the case of the discrete states for this discussion.

Consider a state in the free atom with eigenfunction Ψ_i and eigenenergy E_i [cf. Eq. (2.3a)], which remains discrete (below the conduction band) when the atom chemisorbs, with eigenenergy $E_i + \delta E_i(d)$. By first-order perturbation theory,

$$\delta E_i(d) = \langle \Psi_i | \Delta v | \Psi_i \rangle, \quad (3.1)$$

with

$$\Delta v(\vec{r}) = v_{\text{eff}}[n^{MA}; \vec{r}] - v_{\text{eff}}[n^A; \vec{r}], \quad (3.2)$$

where $n^A(\vec{r})$ is the density in the free atom. (The atomic nuclei for the cases on n^{MA} and n^A are imagined to occupy the same spatial position.) Let us take $n^{MA}(\vec{r}) \approx n^M(\vec{r}) + n^A(\vec{r})$ here. (This crude approximation ignores charge transfer.) Then

$$\Delta v(\vec{r}) \approx v_{\text{es}}[n^M; z] + \Delta v_{\text{xc}}(\vec{r}), \quad (3.3)$$

with

$$\Delta v_{\text{xc}}(\vec{r}) = v_{\text{xc}}[n^M + n^A; \vec{r}] - v_{\text{xc}}[n^A; \vec{r}], \quad (3.4)$$

and with $v_{\text{es}}[n^M; z]$ the electrostatic potential in the bare metal. Now in determining $\langle \Psi_i | \Delta v | \Psi_i \rangle$, let us consider two limiting cases: one in which, over the spatial region important to evaluation of the expectation value, $n^M(\vec{r}) \gg n^A(\vec{r})$, and the opposite case with $n^M(\vec{r}) \ll n^A(\vec{r})$. We expand $\Delta v_{\text{xc}}(\vec{r})$ in powers of $n^A(\vec{r})/n^M(\vec{r})$ (or n^M/n^A), using the fact that in the local-density approximation $v_{\text{xc}}[n; \vec{r}] \approx v_{\text{xc}}(n(\vec{r}))$, and $v_{\text{xc}}(n)$ varies roughly as n^γ , with γ positive but less than unity ($\gamma \approx \frac{2}{3}$). Doing this, and then taking $\langle \Psi_i | \Delta v | \Psi_i \rangle \sim \Delta v(0)$ (recall that the adatom nucleus is at $r = z = 0$ in our coordinate system), shows that the limit $n^M(\vec{r}) \gg n^A(\vec{r})$ (over the relevant region) gives $\delta E_i(d) \sim v_{\text{eff}}[n^M; 0]$ and the opposite limit gives $\delta E_i(d) \sim v_{\text{es}}[n^M; 0]$. It is in this way that we understand the statement that the adatom valence states follow the bare metal "surface potential."

Figure 6 shows the changes with distance in the position and width of the valence resonances for chemisorbed Si and Cl. The Si-3s resonance

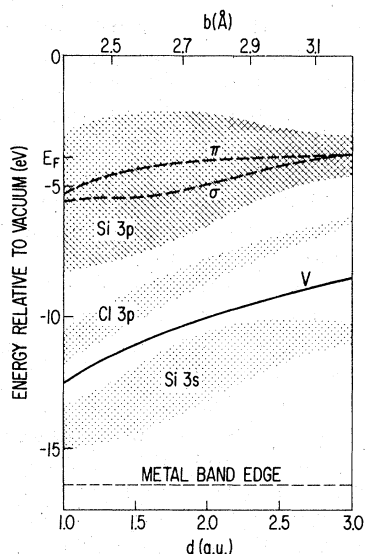


FIG. 6. Characteristics of Si and Cl resonances (cf. Fig. 2) as a function of metal-adatom separation. High-density ($\nu_s = 2$) substrate. Boundaries of shaded regions indicate half-maximum energies. Lower axis d is separation of adatom nucleus from positive background edge (a.u. \equiv bohr). The plane through the outermost nuclei of the substrate represented by this background is half an interplanar spacing behind the background edge. Thus d , the crystal structure of the substrate, and the adsorption site determine an adatom to metal-atom bond length b . The upper axis provides b for a threefold site on a (111) surface of Al as an example. Dashed curves show peak positions for σ ($m=0$) and π ($m=1$) components of Si-3 p resonance. (Not shown for Cl.) Curve V gives effective one-electron potential ($v_{\text{eff}}[n^M; z]$) of bare metal (displaced downward for pictorial reasons).

shows particularly clearly the narrowing at both small and large distances discussed in connection with hydrogen. The asymmetry of the surface potential splits the $m=0$ (σ) and $m=1$ (π) components of the p resonance (recall that m is a good quantum number in the calculation). This splitting is given in the figure for Si. At shorter distances (not shown) the splitting decreases to zero and changes sign.

We expect this reversal of sign of the σ - π splitting with distance to be a general occurrence. If we simply treat the bare-metal surface potential as a perturbation on the free-atom σ and π orbitals (cf. discussion above), then it is seen using first-order perturbation theory that the splitting is proportional to the second derivative of this potential. (The second derivative enters because the σ -orbital samples the potential at z values on either side of the adatom, whereas the π -orbitals sample it for $z \sim 0$. The difference $\langle \sigma | v_{\text{eff}} | \sigma \rangle$

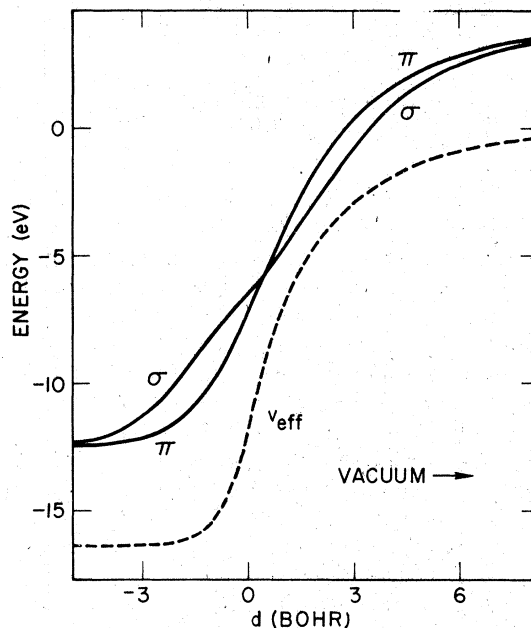


FIG. 7. Simple perturbation calculation of distance dependence of σ - π splitting, using free-atom Si orbitals. The figure shows the energy positions of the otherwise degenerate $3p_\sigma$ and $3p_\pi$ states insofar as they are shifted to first order by the surface potential ($v_{\text{eff}}[n^M; z]$) of a high density ($\nu_s = 2$) metal. The zero of energy for these states has been displaced upward for pictorial convenience. Because of the simplicity of the calculation, these curves are useful only for illustrative purposes; in particular they reproduce the actual results shown in Fig. 6 only qualitatively.

$-\langle \pi | v_{\text{eff}} | \pi \rangle$ is therefore a type of finite-difference approximation to the second derivative.) The second derivative of the potential changes sign,⁴⁵ and thus the sign of the σ - π splitting can be expected to reverse when the adatom is in the vicinity of the inflection point of the potential.

Figure 7 gives the result of such a simple perturbation calculation, using the total effective bare-surface potential $v_{\text{eff}}[n^M; z]$ and free-atom Si $3p$ orbitals. Part of the reason why the splitting in this figure remains perceptible at larger distances than it does in Fig. 6 is the fact that at these distances, it would be more correct in the perturbation calculation to take the surface potential to be only the electrostatic part of v_{eff} (this is the $n^M \ll n^A$ limit, discussed above), whose second derivative drops to zero more rapidly with distance than that of v_{eff} [if $v_{\text{eff}}' \sim e^{-Bz}$, then $v_{\text{eff}}'' \sim e^{-Bz/3}$].

This splitting (and its reversal of sign) is also observed in Fig. 8, which shows the σ and π components of the oxygen $2p$ resonance for two distances. At the larger distance (which is greater

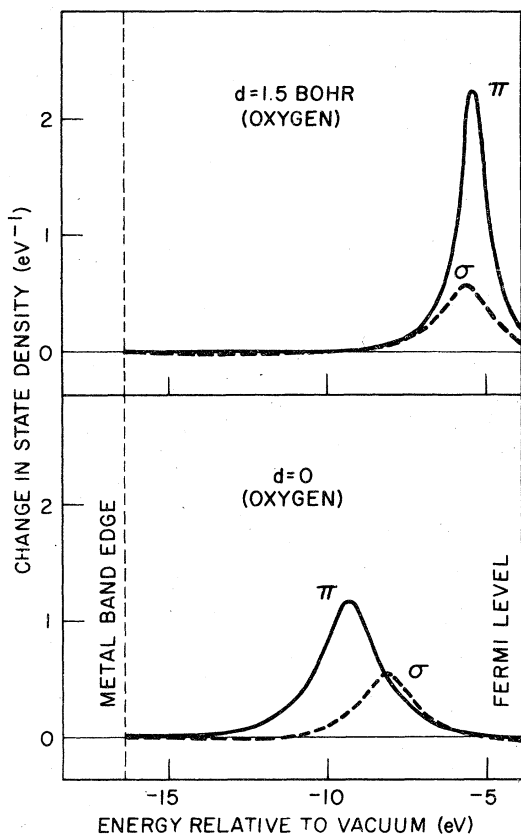


FIG. 8. The σ ($m=0$) and π ($m=1$) components of the state density change $\delta n(E)$ due to chemisorption of oxygen on a high-density ($r_s=2$) substrate. Curves are shown for two different metal-adatom distances d .

than the atom-jellium equilibrium distance), the resonance components are relatively narrow. The π resonance is at a slightly higher energy, as in Si, but the splitting is very small. Closer in, the components broaden, the sign of the σ - π splitting changes, and its magnitude is considerably increased.⁴⁶ A splitting of this order persists to $d \sim -2$ bohrs [the outermost lattice plane for Al(111) would be at $d = -2.2$ bohrs].

We now discuss the dipole moment as a function of distance; this is shown in Fig. 9 for Na, Si, and Cl. (It is useful in thinking about Fig. 9 to keep in mind the density difference maps in Fig. 3.) One can define a "dynamic" charge on the adatom as the slope of such a curve [i.e., $\mu'(d)$].⁴⁷ For distances in the central part of the graph, $\mu'(d)$ is $\sim +0.4$ for Na, ~ -0.5 for Cl and ~ 0 for Si (units are the magnitude of the electron charge). These numbers however do not provide a good measure of static charge transfer because of the importance of other contributions, such as the distance dependence of polarization effects, to

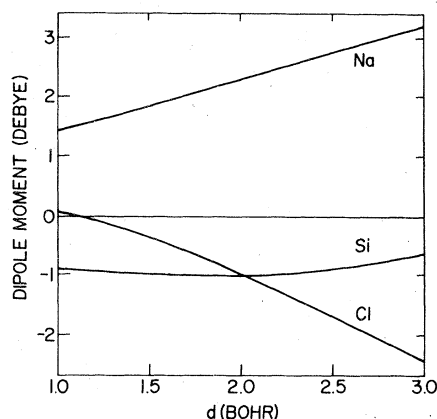


FIG. 9. Dipole moment as a function of metal-adatom distance d for Na, Si, or Cl atom chemisorbed on a high-density ($r_s=2$) substrate. The sign of the dipole moment is defined so that a negative moment corresponds to an increase in substrate work function [see the definition of the dipole moment in Eq. (2.30)].

the value of $\mu'(d)$. This point is discussed in the context of diatomic molecules by Matcha and King.^{48, 49}

Figure 10 shows the way in which the energies of some of the important features of $\delta n(E)$ for chemisorbed oxygen vary with distance. The positions of the two discrete levels (which correspond to the 1s and 2s core levels of the free atom)

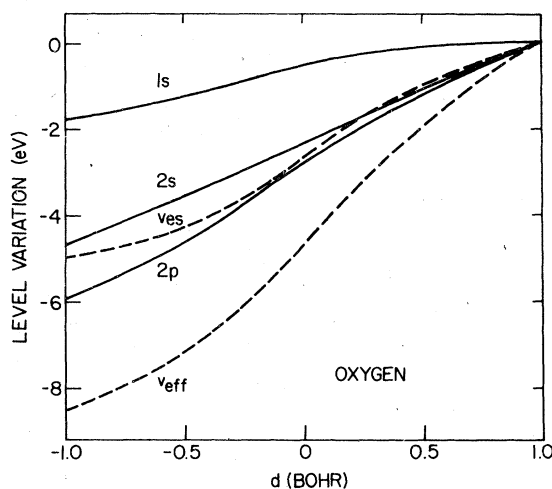


FIG. 10. Variation of the energy positions of the 1s and 2s eigenstates and the peak in the 2p resonance [in $\delta n(E)$] with metal-adatom distance d , for oxygen chemisorbed on a high-density ($r_s=2$) substrate. Shown for comparison are the bare-metal potentials $v_{es}[n^M; z]$ and $v_{eff}[n^M; z]$ evaluated at the position of the adatom nucleus. All curves have been shifted in energy so that they have zero value at the right-hand edge of the graph.

and the position of the peak in the valence resonance (which corresponds to the $2p$ level of the atom) are exhibited. As discussed below, the discrete eigenvalues do not give directly the energy to remove an electron from the corresponding state. However, the *difference* in such excitation energies between the free atom and the chemisorbed atom can be decomposed into a chemical (initial-state) shift and a relaxation (final-state) shift,¹⁶ and the chemical shift is given as the difference in energy eigenvalues between the chemisorbed and free atoms. For these cases, therefore, the curves show the variation with distance of the chemical shift.

The $1s$ level exhibits much less dependence on metal-atom separation than the $2p$ resonance, with the $2s$ level intermediate, though closer to the $2p$, as we would expect from the fact that they have the same principal quantum number. Two important factors affect the distance dependence of the levels, each of which individually would lead to the ordering of the curves seen in the figure. The first arises from the fact that the deeper in energy an orbital lies, the higher is its associated electron density. As discussed earlier, the higher the electron density in the region of a given orbital, the more the orbital eigenvalue will tend to follow the bare-metal electrostatic potential $v_{es}[n^M; z]$ rather than the total bare-metal potential $v_{eff}[n^M; z]$; and v_{es} does not drop as rapidly going into the metal as v_{eff} does. The second factor is a consequence of the fact that as the atom moves into the metal and the valence ($2p$) resonance drops further below the Fermi level, the charge transfer into the valence shell

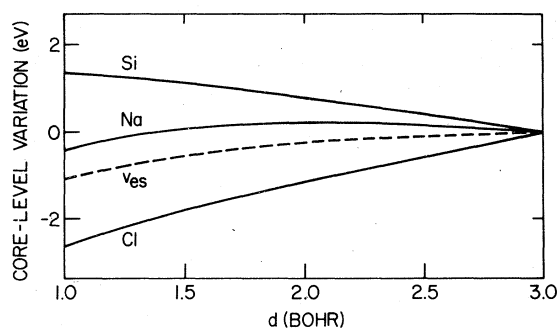


FIG. 11. Variations of the deep core eigenenergies with metal-atom distance d , for Na, Si, and Cl chemisorbed on a high-density ($r_s=2$) substrate. The variations of all of the deep core levels of a given atom are rather similar; the curves actually shown are for the $1s$ level. Included for comparison is the bare-metal potential $v_{es}[n^M; z]$ evaluated at the position of the atom nucleus. All curves have been shifted in energy so that they have zero value at the right-hand edge of the graph.

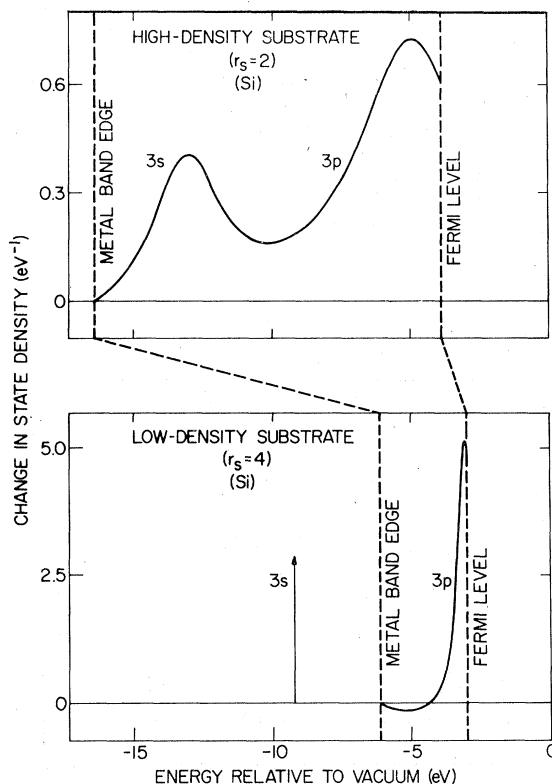


FIG. 12. Comparison between state-density changes $\delta n(E)$ for Si chemisorbed on high ($r_s=2$) and low ($r_s=4$) density substrates. Both curves shown are for an atom taken at a distance $d=1.5$ bohrs. The portions of the curves above the Fermi level are not shown. Note that the $3s$ resonance present in the high-density case becomes a discrete state in the low-density case. The shift of the Fermi-level position relative to vacuum corresponds to a change in the work function when r_s is changed from 2 to 4 (see Ref. 25).

can be expected to increase. Simple electrostatic considerations indicate that this added charge will raise the electrostatic energy of orbitals concentrated near the nucleus ($1s$) more than it will raise the electrostatic energy of orbitals comparable in size to the valence shell ($2s$, and $2p$ itself).

In Fig. 11, we exhibit the variation of deep-core eigenenergies with distance for Na, Si, and Cl. In contrast to the Si- $3s$ resonance in Fig. 6, the deep Si core levels do not drop as the atom is moved closer to the metal but in fact rise slightly. We ascribe this difference to the effect of increased charge transfer into the Si $3p$ shell as the atom is moved closer (which occurs because the $3p$ resonance moves gradually down through the Fermi level, as seen in Fig. 6). As noted above, this charge transfer affects the positions of deep levels most strongly. It is apparently large

enough to counterbalance the effect of the drop in bare-metal potential over the range of distances shown. This discussion suggests that the rather different behavior of Cl arises simply from the fact that since its valence resonance is always well below the Fermi level (Fig. 6), there is rather little change in charge transfer with distance.

Finally, we show in Fig. 12 an example of the effect of changing the substrate density.⁵⁰ The top part of the figure gives the state-density difference $\delta n(E)$ for Si on an $r_s = 2$ (\sim Al density) substrate for energies between the bottom of the metal conduction band and the Fermi level. (The adatom is placed at a distance $d = 1.5$ bohrs.) The bottom part of the figure gives $\delta n(E)$ for Si on an $r_s = 4$ (\sim Na density) substrate, over the same energy range and with the distance d unchanged. Since the density of metal states seen by the $3p$ resonance is so much lower in this case, the resonance is much narrower. Furthermore, the metal band edge lies above the $3s$ state, so this state is no longer broadened, but remains discrete when the atom chemisorbs, as the deeper core states do.

We conclude this section by discussing some of the important considerations that arise if we wish to compare the results calculated using the atom-jellium model with experimental data for low-coverage chemisorption. The first important point is that on an actual metal surface, the metal-adatom separation at favorable adsorption sites will be somewhat smaller than the value obtained in the atom-jellium model. This fact is suggested by a simple hard-sphere model of the substrate atoms (recalling that the positive-background edge is half an interplanar spacing in front of the outermost lattice plane); and it is demonstrated in Appendix D, in which the discrete substrate lattice is reintroduced using first-order perturbation theory. The perturbation $\delta v(\vec{r})$ in this case is the difference between the total lattice pseudopotential and the potential due to the semi-infinite positive background.

The atomic binding energy ΔE_a associated with the most favorable adsorption sites is in general somewhat larger than the value for the atom-jellium model, as seen in Appendix D. Although the change in energy of the adatom core (which is concentrated spatially and often has several units of net charge) due to the perturbation $\delta v(\vec{r})$ can be large, the effect of this perturbation on individual electron states, particularly when it is averaged over the relatively diffuse valence orbitals, is usually quite small. Because of this, we expect that $\delta n(E)$ for the adatom in the presence of the pseudopotential lattice will be similar

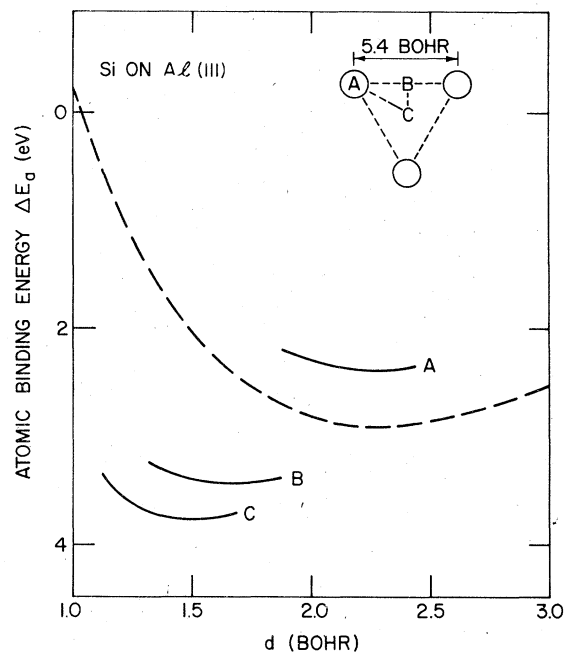


FIG. 13. The dashed curve gives the atomic binding energy (see definition in Sec. II) as a function of distance for Si chemisorbed on an $r_s = 2$ jellium substrate. The solid curves give the binding energy when the pseudopotential correction $\delta \Delta E_a$ [Eq. (D7)] is added to the result for the atom-jellium model. These corrections are computed for adsorption on the (111) face of Al at three possible sites: on top of a substrate atom (A), bridge position (B), and centered position over a hole in the second layer of atoms (C). Note that the outermost plane of substrate nuclei lies half an interplanar spacing behind the positive background edge (corresponding to $d = -2.2$ bohrs in the present case). The equilibrium position for adsorption in the centered site C corresponds to an Al-Si bond length of 2.6 Å (see text).

to $\delta n(E)$ for the atom-jellium model evaluated at the reduced metal-adatom separation. Graphs such as Figs. 5 or 6 are appropriate for this evaluation. [Note that the top half of Fig. 12 gives $\delta n(E)$ for Si evaluated at the centered-site (C) equilibrium distance shown in Fig. 13.] Instead of obtaining the metal-adatom separation from a total-energy evaluation as described in Appendix D, it could of course be estimated using hard-sphere radii (Appendix D also gives an example of this), or, e.g., obtained from the analysis of a low-energy electron diffraction experiment. The dipole moment appropriate to the reduced metal-adatom separation can be estimated from atom-jellium values (shown in Fig. 9 for Na, Si, and Cl), but this neglects further polarization of the adatom charge distribution by the discrete lattice potential.

There is a further point to be made concerning

the relation between the eigenvalues E_i of Eq. (2.3a) [the change in spectral distribution of which gives $\delta n(E)$] and actual excitation energies that would be measured in a photoemission experiment. Now it is rigorously true that these eigenvalues are derivatives of the total energy of the system with respect to orbital occupation number n_i ^{16,21}: $E_i = \partial E_{\text{tot}} / \partial n_i$. The eigenvalue for a discrete state is therefore not an actual excitation energy, but can be thought of as the energy required to remove an infinitesimal fraction of an electron to vacuum. This difference is quite important for the very localized deep-core states, but it becomes less and less important as the state becomes delocalized. In particular, the difference appears not to be large for valence resonances of the type shown, e.g., in Fig. 2, and currently available evidence suggests that the peaks in the $\delta n(E)$ defined in this paper should correspond reasonably closely to peak positions observed in photoemission, especially in the case of resonances which are not extremely narrow.^{2, 52}

We note in this connection a somewhat unusual property of the 3s state shown in the bottom part of Fig. 12. In this case, the (negative of the) energy eigenvalue and the directly computed excitation energy are nearly identical: the eigenvalue (as seen in the figure) lies 9.2 eV below the vacuum level, while the energy to remove an electron is 9.4 eV. In general, the excitation energy is given by the (negative of the) average of E_i as it varies with removal of an electron from the state.⁵³ In this case, the metallic screening charge distribution built up is similar to that of the 3s electron removed, and thus the total electron density does not vary appreciably with this removal. The eigenvalue is therefore approximately unchanged, and equal to the (negative of the) excitation energy. The similarity of the electron density being removed to that being replaced by the screening process exemplifies the ideas developed in Ref. 16; in the present context, they suggest that the screening charge is well described by the density distribution of a Si 3p orbital, which in turn is very similar to that of a 3s orbital.

ACKNOWLEDGMENTS

We are delighted to thank J. F. Janak, F. Forstmann, D. W. Jepsen, M. C. Gutzwiller, C. D. Gelatt, Jr., J. E. Demuth, D. E. Eastman, P. M. Marcus, and H. F. Budd for a number of very useful conversations about this work.

APPENDIX A: OBTAINING $\Psi_{E_{mi}}^{M(A)}$ AND $\Psi_{E_{cm}}^{MA}$

The fundamental solutions $\Psi_{E_{mi}}^{M(A)}(\vec{r})$ appearing in Sec. II were constructed using the phase-function

technique described by Williams and Morgan.³² These solutions are represented as an r -dependent linear combination of free-particle solutions (we will drop the superscripts M and MA here):

$$\Psi_{E_{mi}}(\vec{r}) = \sum_{l'=|m|}^{\infty} [C_{E_{mi}l'}(r)j_{l'}(pr) + S_{E_{mi}l'}(r)h_{l'}^+(pr)]Y_{l'm}(\Omega). \quad (\text{A1})$$

Here $p = \sqrt{E}$, and $j_{l'}$ and $h_{l'}^+$ are the spherical Bessel functions described by Messiah.⁵⁴ A reference energy with respect to which core-state energies are negative is convenient; we take the vacuum level as our reference. In this case, $j_{l'}(pr)$ grows exponentially at large r and $h_{l'}^+(pr)$ decays, for E below the vacuum level. Just as the l sum of Eq. (2.19) is limited by an $l_{\text{max}} (\sim 6)$ in the actual calculation, so also was the sum in Eq. (A1) limited (using the same value of l_{max}).

Representing the solutions as in Eq. (A1) has several implications. First, as seen in Ref. 32, each single-particle equation (2.3a) takes the form of a system of coupled first-order linear ordinary differential equations⁵⁵ for C and S :

$$\frac{dC_{E_{mi}l'}(r)}{dr} = pr^2 h_{l'}^+(pr) \int d\Omega Y_{l'm}^*(\Omega) \times v_{\text{eff}}[n; \vec{r}] \Psi_{E_{mi}}(\vec{r}), \quad (\text{A2})$$

with a similar equation for S in which $h_{l'}^+$ is replaced by $-j_{l'}$.⁵⁶ Second, the defining behavior at small r [Eq. (2.17)] is easily specified as an initial condition for outward radial integration:

$$C_{E_{mi}l'}(0) = (2l+1)!! p^{-l} \delta_{ll'}, \quad S_{E_{mi}l'}(0) = 0. \quad (\text{A3})$$

Let us now consider the calculation of the adatom core states $\Psi_{E_{cm}}$ within this framework. At sufficiently large radii $R \gg |E_c|^{1/2}$, the core-state wave function is unaffected by the details of the potential, and so we can set $v_{\text{eff}} \equiv 0$ for $r > R$ in calculating these states. The core-state energies are then taken to be the energies at which

$$\det[C_{E_{cm}l'}(R)] = 0, \quad (\text{A4})$$

where the determinant is taken with respect to the l, l' indices ($|m| \leq l, l' \leq l_{\text{max}}$). This condition states that at the energy E_c there exists a linear combination of the fundamental solutions $\Psi_{E_{cm}l}$,

$$\Psi_{E_{cm}}(\vec{r}) = \sum_{l=|m|}^{\infty} \beta_{E_{cm}l} \Psi_{E_{cm}l}(\vec{r}), \quad (\text{A5})$$

(with the sum limited to l_{max} in the actual calculation), which is exponentially decaying in all directions at large r . (That is, the admixture of functions $j_{l'}$ in $\Psi_{E_{cm}}$ drops to zero at large distances, leaving only functions $h_{l'}^+$.) The core-level energies are found by counting the number of

times the quantity

$$\det[C_{E_{mi}l'}(r)]$$

passes through zero in the course of the outward radial integration (from $r=0$ to $r=R$) and locating the energy E_c for which this number of nodes increases by one.

APPENDIX B: REDUCED BARE-METAL GREEN'S FUNCTION $G_{E_{mi}}^M(r, \theta)$

Let us substitute expression (2.21) for $G_E^M(\vec{r}, \vec{r}')$ into the definition of $G_{E_{mi}}^M(r, \theta)$ [(2.26)]. (Since these equations show that only the sign of $G_{E_{mi}}^M$ is changed when m is replaced by $-m$, we will consider just $m \geq 0$ here.) Then we see (using the coordinate systems of Fig. 1) that³⁶

$$\begin{aligned} G_{E_{mi}}^M(r, \theta) &= \frac{1}{2\pi} \int_0^\infty d\kappa \kappa J_m(\kappa r \sin\theta) W_{E\kappa}^{-1} \\ &\quad \times [\Theta(\theta - \frac{1}{2}\pi) \bar{u}_{E\kappa}^M(r \cos\theta) \alpha_{E_{m\kappa}l}^M \\ &\quad + \Theta(\frac{1}{2}\pi - \theta) u_{E\kappa}^M(r \cos\theta) \bar{\alpha}_{E_{m\kappa}l}^M] \end{aligned} \quad (B1)$$

(with $0 \leq \theta \leq \pi$), where the coefficients α^M are given by

$$\begin{aligned} \alpha_{E_{m\kappa}l}^M &= c_{lm} \lim_{r' \rightarrow 0} r'^{-1} \int_{-1}^1 d \cos\theta' P_l^m(\cos\theta') \\ &\quad \times J_m(\kappa r' \sin\theta') u_{E\kappa}^M(r' \cos\theta') \end{aligned} \quad (B2)$$

with a corresponding expression for $\bar{\alpha}^M$ in terms of \bar{u}^M . The coefficient c_{lm} here is

$$c_{lm} = [\pi(2l+1)(l-m)!/(l+m)!]^{1/2}. \quad (B3)$$

[It is easily seen that the $\alpha_{E_{m\kappa}l}^M$ above is identical to the corresponding coefficient in Eq. (2.18).⁵⁷]

We now write a Taylor series for $u_{E\kappa}^M$ and $\bar{u}_{E\kappa}^M$ about the origin:⁵⁸

$$\begin{aligned} u_{E\kappa}^M(z) &= \sum_{n=0}^{\infty} \frac{z^n}{n!} \frac{d^n}{dz^n} u_{E\kappa}^M(z') \Big|_{z'=0} \\ &= \exp\left(z \frac{d}{dz'}\right) u_{E\kappa}^M(z') \Big|_{z'=0} \end{aligned} \quad (B4)$$

and similarly for \bar{u}^M . Now define the function

$$\begin{aligned} F_{lm}(\mu, \lambda) &= \lim_{r \rightarrow 0} r^{-1} \int_{-1}^1 d \cos\theta e^{\lambda r \cos\theta} \\ &\quad \times J_m(\mu r \sin\theta) P_l^m(\cos\theta). \end{aligned} \quad (B5)$$

Then we can write

$$\alpha_{E_{m\kappa}l}^M = c_{lm} F_{lm}\left(\kappa, \frac{d}{dz'}\right) u_{E\kappa}^M(z') \Big|_{z'=0}, \quad (B6)$$

with a similar relation for $\bar{\alpha}^M$ in terms of \bar{u} .

To obtain an explicit expression for $F_{lm}(\mu, \lambda)$, we use a result due to Gegenbauer, as given by Watson:⁵⁹

$$\begin{aligned} \int_0^\pi e^{i\kappa \cos\theta \cos\psi} J_{\nu-1/2}(z \sin\theta \sin\psi) \\ \times C_\nu^{\nu}(\cos\theta) \sin^{\nu+1/2}\theta d\theta \\ = \left(\frac{2\pi}{z}\right)^{1/2} i^\nu \sin^{\nu-1/2}\psi C_\nu^{\nu}(\cos\psi) J_{\nu+\nu}(z). \end{aligned} \quad (B7)$$

With appropriate changes of variable, and use of the explicit form of the Gegenbauer polynomials⁶⁰ and the binomial theorem, we have (recalling the relation between the Gegenbauer polynomials and the associated Legendre function⁶⁰)

$$F_{lm}(\mu, \lambda) = \sum_{n=0}^{[(l-m)/2]} \sum_{k=0}^n b_{klmn} \mu^{2k+m} \lambda^{l-m-2k}, \quad (B8)$$

where $[x]$ is the greatest integer in x and where

$$b_{klmn} = \frac{(-1)^{k+m+n} (2l-2n-1)!!}{2^{n-1} (2l+1)!! (l-m-2n)! (n-k)! k!} \quad (B9)$$

with $(-1)!!$ defined to be unity.

We see therefore that

$$\begin{aligned} \alpha_{E_{m\kappa}l}^M &= c_{lm} \sum_{n=0}^{[(l-m)/2]} \sum_{k=0}^n b_{klmn} \kappa^{2k+m} \\ &\quad \times \frac{d^{l-m-2k}}{dz'^{l-m-2k}} u_{E\kappa}^M(z') \Big|_{z'=0} \end{aligned} \quad (B10)$$

and similarly for $\bar{\alpha}^M$ in terms of \bar{u}^M . These expressions for α^M and $\bar{\alpha}^M$ permit the most convenient numerical evaluation of Eq. (B1) for $G_{E_{mi}}^M(r, \theta)$. Second and higher derivatives of $u_{E\kappa}^M(z)$ were obtained, using Eq. (2.22), from the values of $u_{E\kappa}^M(0)$ and $du_{E\kappa}^M(z)/dz|_{z=0}$ and derivatives of the bare-metal potential (similarly for \bar{u}^M). The integral in Eq. (B1) was carried to large enough values of κ to yield convergence.⁶¹

APPENDIX C: LONG-RANGE CHARGE DISTURBANCES

As described in the text, the electron-density distribution in the metal-adatom system is computed only within a sphere of radius R about the nucleus. There are, however, long-range charge disturbances outside the sphere which, while small, must be at least approximately taken into account in the calculation of quantities such as the dipole moment which emphasize charges distant

from the adatom nucleus.

These charge disturbances have both a direct and an indirect effect on the values of the various computed quantities, in the following sense: The charge disturbance outside the sphere makes a contribution of its own to (for example) the dipole moment that should be added to the moment calculated for the charge within the sphere, and in addition makes a contribution to the potential felt by the electron distribution within the sphere which in turn affects the dipole moment of this disturbance when it is included in the self-consistency cycle.⁶²

We have dealt with charge disturbances outside the sphere in the following approximate way. We have identified what we believe to be the two dominant components of these disturbances, approximated them by analytic forms, and used these forms to obtain the effect of these disturbances on the quantities of interest. The indirect effect is generally found to be somewhat less important than the direct effect, but it is included by using the analytic forms to approximate the contribution of the charges outside the sphere to the potential within the sphere that determines the electron wave functions. We can test our procedures by examining the stability of our results with respect to changes in the sphere radius R . This test both confirms the necessity of taking into account the long-range charge disturbances, and shows that our approximate treatment is of adequate accuracy to do this.⁶³ The two dominant long-range components of $\delta n(\mathbf{r}, \theta)$ are the Friedel oscillations extending into the bulk of the metal which are induced by the presence of the adatom, and a charge distribution confined to the surface that can be considered to be induced essentially by the dipole field in the vacuum arising from the distribution of charges within the sphere.⁶⁴ We

describe below the analytic forms we have used for these long-range charge disturbances, and discuss their direct contribution to the dipole moment, since it is for this case that their inclusion is found to be most important. The calculation of the direct contribution to the force on the nucleus, and to the potential within the sphere (which in turn produces the indirect effect mentioned above on all computed quantities), proceeds in a similar manner. We also note briefly the calculation of the direct contribution to the adatom binding energy, which in leading approximation does not depend on the actual form of the long-range charge disturbances, but only on the total charge contained in them.

An asymptotic analysis of Eq. (2.1) in conjunction with Eqs. (2.27) and (2.28) indicates that the leading term in the Friedel-oscillation contribution to the density disturbance outside the sphere should have the form^{36, 65}

$$\delta n_F(\mathbf{r}, \theta) = \frac{A(\theta) \cos[2k_F r + \alpha(\theta)]}{(2k_F r)^3} \times \Theta(z_F - r \cos \theta) \Theta(r - R), \quad (C1)$$

where we will consider for discussion just the case $-R < z_F < 0$. The first step function in this equation is inserted to restrict the use of the approximate expression for the density disturbance to a region where it is theoretically justified.⁶⁶ This implies the neglect of contributions from the immediate surface region to the (already small) effect. The amplitude $A(\theta)$ and phase $\alpha(\theta)$ were obtained by fitting this form for $\delta n_F(\mathbf{r}, \theta)$ to the actual computed $\delta n(\mathbf{r}, \theta)$ just inside the sphere surface on each iteration. The contribution of this charge to the dipole moment defined in Eq. (2.30) is given by

$$\begin{aligned} \mu_F &= - \lim_{z \rightarrow -\infty} \int_{z > z} d^3 r z \delta n_F(\mathbf{r}, \theta) \\ &= \frac{\pi}{8k_F^4} \lim_{z \rightarrow -\infty} \left(\int_{-1}^{z_F/R} A(\theta) \cos \theta \sin[2k_F R + \alpha(\theta)] d \cos \theta + \int_{z_F/R}^0 A(\theta) \cos \theta \sin \left[\frac{2k_F z_F}{\cos \theta} + \alpha(\theta) \right] d \cos \theta \right. \\ &\quad \left. - \int_{-1}^0 A(\theta) \cos \theta \sin \left[\frac{2k_F z}{\cos \theta} + \alpha(\theta) \right] d \cos \theta \right). \end{aligned} \quad (C2)$$

In accordance with the fact that we have taken only the leading term [in powers of $(2k_F R)^{-1}$] in the expression for $\delta n_F(\mathbf{r}, \theta)$, we drop the second term on the right-hand side of the above equation, since it is easily seen to be $O((2k_F R)^{-1})$ relative to the first term. The third term vanishes in the limit $z \rightarrow -\infty$, and thus

$$\mu_F = \frac{\pi}{8k_F^4} \int_{-1}^{z_F/R} A(\theta) \cos \theta \sin[2k_F R + \alpha(\theta)] d \cos \theta. \quad (C3)$$

We see from this the necessity for taking μ_F into account—simply making R very large does not cause μ_F to be small, since the magnitude of μ_F

does not decrease as R increases (it only oscillates).⁶⁷

Now let us discuss the surface-region charge distribution $\delta n_s(\mathbf{r}, \theta)$ outside the sphere induced by the electrostatic field due to the charges within the sphere. We consider that R has been taken to be large enough compared with the thickness of this surface charge distribution⁶⁸ to justify neglect of the thickness, and thus we can take $\delta n_s(\mathbf{r}, \theta)$ to be confined to a plane at $z = z_s$ (the location of the computed center of gravity of screening charge induced on a jellium surface by a uniform weak electric field.⁶⁸) We take for purposes of discussion only the case $-R < z_s < 0$ and $z_s < z_{cg}$ (the location of the center of gravity of the electronic charge within the sphere). We also consider that R has been chosen large enough that $R \gg |z_{cg}|$.

Let us now consider the perpendicular component of the electric field on the plane $z = z_s$ at a distance r ($>R$) from the nucleus, due to the charges within the sphere. These charges consist of the nucleus of charge Z and a distribution of Q_R electronic charges. If we perform a multipole expansion for the field due just to the electronic charge within the sphere about its center of gravity, there will be no dipolar field and if we drop higher multipoles, then this charge will give rise to a field component $2Q_R(z_{cg} - z_s) \times (r^2 - 2z_{cg}z_s + z_{cg}^2)^{-3/2} \approx 2Q_R(z_{cg} - z_s)/r^3$. (The factor of 2 arises from the use of rydbergs). The nucleus contributes a field component $2Zz_s/r^3$. Since the surface charge distribution $\delta n_s(\mathbf{r}, \theta)$ screens out the field within the metal, the Gauss theorem implies that⁶⁹

$$\delta n_s(\mathbf{r}, \theta) = -\frac{1}{2\pi r^3} [Zz_s - Q_R(z_s - z_{cg})] \times \delta(r \cos \theta - z_s) \Theta(r - R). \quad (C4)$$

Note that if the nucleus were replaced by a weak point charge far from the surface, we would have $z_{cg} = z_s$, causing the second term here to vanish, and $\delta n_s(\mathbf{r}, \theta)$ would reduce to a simple image form.⁹ The contribution to the dipole moment defined in Eq. (2.30) that is associated with δn_s is

$$\mu_s = -\int d^3r z \delta n_s(\mathbf{r}, \theta) = \frac{z_s}{R} [Zz_s - Q_R(z_s - z_{cg})]. \quad (C5)$$

We now briefly consider the direct contribution of the charge disturbances outside the sphere to the calculated atomic binding energy ΔE_a (the indirect contribution is taken into account by inclusion of the potential due to δn_F and δn_s in the self-consistency loop). Since the sphere is chosen large enough to insure that the charge q in disturbances outside the sphere is small, we consider

corrections to the energy of $O(q)$ only, dropping those of $O(q^2)$. Then it can be shown⁷⁰ that the correction to the calculated atomic binding energy (with the vacuum potential taken to be the zero when the electrostatic part of this energy is calculated) is

$$\Delta E_a^q \approx q\Phi, \quad (C6)$$

where Φ is the bare-metal work function. Since $q = Z - Q_R$ (because the nuclear charge is completely screened at large distances), this leading correction to the atomic binding energy has the convenient simplicity that it can be computed without using the forms for the charge disturbances outside the sphere.

APPENDIX D: REINTRODUCING THE DISCRETE SUBSTRATE LATTICE

We discuss in this Appendix the reintroduction of the discrete lattice of the substrate into the atom-jellium model, using pseudopotential perturbation theory. Consider a model of the substrate in which the ions are represented by pseudopotentials situated on the sites of a regular semi-infinite lattice.⁷¹ Let $\delta v(\vec{r})$ be the difference between the total pseudopotential and the potential due to the semi-infinite positive background employed in the atom-jellium model to represent the ionic lattice. We will use first-order perturbation theory to calculate the change in energy (relative to the value obtained in the atom-jellium model) due to the perturbation $\delta v(\vec{r})$.

The new value of the total energy now depends not only on the metal-adatom separation but also on the lateral position of the adatom. The spatial position which minimizes the energy will generally correspond to a metal-adatom separation smaller than that found for the atom-jellium model, and the atomic binding energy will be somewhat larger.

By employing first-order perturbation theory, we avoid the difficult problem of solving the truly three-dimensional single-particle equations appropriate to the metal-adatom system with a discrete lattice.^{17, 20} Perturbation theory has been used in this way by Lang and Kohn²⁵ to study work-function anisotropies and surface energies in simple metals. It is generally successful for relatively close-packed surfaces,⁷² failing only in a case such as Pb, which is known to have a particularly strong pseudopotential.⁷³ The importance of discrete lattice effects in the present context was recognized by Gunnarsson, Hjelmberg, and Lundqvist.^{18, 19}

We will use the local ion pseudopotential proposed by Ashcroft,⁷⁴ which has the form³⁶

$$v_{ps}(\vec{r}) = -(2Z_{ion}/r)\Theta(r - r_c), \quad (D1)$$

where Z_{ion} is the ionic charge and r_c is a cutoff radius determined for each metal to give a good description of bulk properties. (The factor of 2 arises because of the use of rydbergs.)

We now describe the computation of $\delta v(\vec{r})$ using this pseudopotential; the substrate lattice will be assumed to be cubic. Let N_s be the number of rectangular sublattices in each substrate lattice plane; and let N_p be the number of inequivalent planes [for fcc (111), e.g., $N_s=2$ and $N_p=3$]. Let us label the successive equivalent planes by the integer n , running from -1 for the plane closest to the surface to $-\infty$; and let us use an index ν (running from 1 to $N_s N_p$) to label each of a given one of the N_s sublattices in a given one of the N_p inequivalent lattice planes. To label the sites on each two-dimensional rectangular sublattice, we use the integers l and m , running from $-\infty$ to $+\infty$. The positive background which represents the ionic lattice in the atom-jellium model fills the half space $z < -d$ (see Fig. 1); the outermost lattice plane of the ionic lattice represented by this background will then be at $z = -\frac{1}{2}D - d$, where D is the (smallest) interplanar spacing.⁹

In terms of the coordinates of a point $\vec{r} = (x, y, z)$, let us define

$$\begin{aligned} X_\nu &= (\alpha a)^{-1}x - C_\nu^X, \\ Y_\nu &= (\beta a)^{-1}y - C_\nu^Y, \\ Z_\nu &= (\gamma a)^{-1}z - C_\nu^Z, \end{aligned} \quad (\text{D2})$$

where a is the lattice constant, and where α, β, γ , and the constants C are such that when \vec{r} is at a lattice site, $(X_\nu, Y_\nu, Z_\nu) = (l, m, n)$ (with l, m , and n taking on the range of values noted above). For the fcc (111) case, for example, $\alpha = \frac{1}{2}\sqrt{6}$, $\beta = \frac{1}{2}\sqrt{2}$, $\gamma = \sqrt{3}$.

It is convenient to split the perturbing potential into a pure Coulomb part and a part representing the pseudopotential cancellation in the cores:

$$\delta v(\vec{r}) = \delta v_{\text{Coul}}(\vec{r}) + \delta v_{\text{cores}}(\vec{r}), \quad (\text{D3})$$

where the two terms are then given by

$$\delta v_{\text{Coul}}(\vec{r}) = -\frac{2Z_{\text{ion}}}{a} \sum_{n=-\infty}^{-1} \sum_{\nu=1}^{N_s N_p} \sum_{l, m=-\infty}^{\infty} R_{l m n \nu}^{-1} - v_+(\vec{r}), \quad (\text{D4})$$

with $v_+(\vec{r})$ the electrostatic potential due to the semi-infinite positive background and

$$R_{l m n \nu} \equiv [\alpha^2(l - X_\nu)^2 + \beta^2(m - Y_\nu)^2 + \gamma^2(n - Z_\nu)^2]^{1/2}, \quad (\text{D5})$$

and by

$$\begin{aligned} \delta v_{\text{cores}}(\vec{r}) &= \frac{2Z_{\text{ion}}}{a} \sum_{n=-\infty}^{-1} \sum_{\nu=1}^{N_s N_p} \sum_{l, m=-\infty}^{\infty} R_{l m n \nu}^{-1} \\ &\quad \times \Theta\left(\frac{r_c}{a} - R_{l m n \nu}\right). \end{aligned} \quad (\text{D6})$$

The change in atomic binding energy is

$$\delta \Delta E_a = Z \delta v_{\text{Coul}}(0) - \int d^3r \delta n(\vec{r}) \delta v(\vec{r}), \quad (\text{D7})$$

where Z is the adatom nuclear charge and $\delta n(\vec{r})$ is given in Eq. (2.28).

For a given \vec{r} , at most one term of the summation in Eq. (D6) will contribute,⁷⁵ and so the difficulty in evaluating $\delta v(\vec{r})$ is isolated in the pure Coulomb sum in Eq. (D4). The evaluation of $\delta v_{\text{Coul}}(\vec{r})$ proceeds in the same way as the evaluation of the Coulomb sums in Appendix C of Ref. 25 and thus we only give the result, in terms of the functions F, G , and H defined in that Appendix:

$$\begin{aligned} \delta v_{\text{Coul}}(\vec{r}) &= -\frac{2Z_{\text{ion}}}{a} \sum_{n=-\infty}^{-1} \sum_{\nu=1}^{N_s N_p} \left[\sum_{l, m=-\infty}^{\infty} F(\alpha(l - X_\nu), \beta(m - Y_\nu), \gamma(n - Z_\nu), \eta) \right. \\ &\quad + (2\alpha\beta)^{-1} \sum_{l, m=-\infty}^{\infty} \cos 2\pi l X_\nu \cos 2\pi m Y_\nu G\left(\gamma(n - Z_\nu), \frac{l}{\alpha}, \frac{m}{\beta}, \eta\right) \\ &\quad \left. + (\alpha\beta)^{-1} H(\gamma|n - Z_\nu|, \eta) \right] - 4\pi\bar{n} (|\lambda| - \frac{1}{2}D)^2 \Theta(-z - d), \end{aligned} \quad (\text{D8})$$

where \bar{n} is the positive background density and λ is the distance to the nearest lattice plane, and where the prime on the summation in the second term indicates the exclusion of the $l=m=0$ term. The quantity η is a convergence parameter which is chosen for equally rapid convergence of all

terms ($\eta^2 \sim \pi$). Including only the first few terms in the infinite summations generally gives quite accurate results.

As an example of binding energy curves that include the lattice pseudopotential correction, we give in Fig. 13 results for Si adsorbed on the

(111) face of Al.⁷⁶ The most favorable adsorption site is seen to be the centered site (over a hole in the second layer of atoms),⁷⁷ which seems intuitively reasonable.⁷⁸ Note the way in which the distance d for adsorption at this site is decreased, and the atomic binding energy increased, relative to the atom-jellium model. Recalling again that d is measured from a point half an interplanar spacing in front of the outermost lattice plane,⁹ we find the Al-Si bond length for adsorption at this site to be 2.6 Å. Marcus *et al.*⁷⁹ suggest, from analysis of experimental

data, that the bond length for a case such as this should be the sum of the covalent radius of the adatom and the metallic radius⁸⁰ of the substrate. For Si-Al, this is 2.60 Å,⁸¹ which indicates that our calculated bond length is reasonable. The first-order pseudopotential calculation appears to give generally reasonable results, but there is evidence that it is not adequate in every case: this treatment shows that for Cl-Al(111), site A in Fig. 13 is energetically more favorable than site C,⁸² which seems intuitively unlikely.⁸³

- ¹T. B. Grimley, in *Electronic Structure and Reactivity of Metal Surfaces*, edited by E. G. Derouane and A. A. Lucas (Plenum, New York, 1976), p. 35.
- ²J. R. Schrieffer, *J. Vac. Sci. Technol.* **9**, 561 (1972); **13**, 335 (1976); and in *Dynamic Aspects of Surface Physics*, edited by F. O. Goodman (Editrice Compositori, Bologna, 1974), p. 250.
- ³R. Gomer, *Crit. Rev. Solid State Sci.* **4**, 247 (1974); and in *Solid State Physics*, edited by F. Seitz, D. Turnbull, and H. Ehrenreich (Academic, New York, 1975), Vol. 30, p. 93.
- ⁴J. W. Gadzuk, in *Surface Physics of Materials*, edited by J. M. Blakely (Academic, New York, 1975), Vol. II, p. 339.
- ⁵B. I. Lundqvist, H. Hjelmberg, and O. Gunnarsson, in *Photoemission and the Electronic Properties of Surfaces*, edited by B. Feuerbacher, B. Fitton, and R. F. Willis (Wiley, New York, 1978), p. 227.
- ⁶P. Hohenberg and W. Kohn, *Phys. Rev.* **136**, B864 (1964).
- ⁷W. Kohn and L. J. Sham, *Phys. Rev.* **140**, A1133 (1965).
- ⁸L. Hedin and S. Lundqvist, in *Solid State Physics*, edited by F. Seitz, D. Turnbull, and H. Ehrenreich (Academic, New York, 1969), Vol. 23, p. 1.
- ⁹N. D. Lang, in *Solid State Physics*, edited by F. Seitz, D. Turnbull, and H. Ehrenreich (Academic, New York, 1973), Vol. 28, p. 225.
- ¹⁰J. A. Appelbaum and D. R. Hamann, *Rev. Mod. Phys.* **48**, 479 (1976).
- ¹¹O. Gunnarsson and B. I. Lundqvist, *Phys. Rev. B* **13**, 4274 (1976); O. Gunnarsson, J. Harris, and R. O. Jones, *J. Chem. Phys.* **67**, 3970 (1977).
- ¹²V. L. Moruzzi, A. R. Williams, and J. F. Janak, *Phys. Rev. B* **15**, 2854 (1977); J. F. Janak and A. R. Williams, *Phys. Rev. B* **14**, 4199 (1976).
- ¹³N. D. Lang, *Phys. Rev. B* **4**, 4234 (1971).
- ¹⁴N. D. Lang and A. R. Williams, *Phys. Rev. Lett.* **34**, 531 (1975).
- ¹⁵N. D. Lang and A. R. Williams, *Phys. Rev. Lett.* **37**, 212 (1976).
- ¹⁶N. D. Lang and A. R. Williams, *Phys. Rev. B* **16**, 2408 (1977).
- ¹⁷In re H-Si, see J. A. Appelbaum and D. R. Hamann, *Phys. Rev. Lett.* **34**, 806 (1975); J. A. Appelbaum, D. R. Hamann, and K. H. Tasso, *ibid.* **39**, 1487 (1977).
- ¹⁸O. Gunnarsson, H. Hjelmberg, and B. I. Lundqvist, *Phys. Rev. Lett.* **37**, 292 (1976); *Surf. Sci.* **63**, 348 (1977).
- ¹⁹H. Hjelmberg, O. Gunnarsson, and B. I. Lundqvist, *Surf. Sci.* **68**, 158 (1977).
- ²⁰Some calculations use a film or slab substrate, which is several layers thick, but infinite in two directions. In re N-Cu, see J. R. Smith, F. J. Arlinghaus, and J. G. Gay, *Solid State Commun.* **24**, 279 (1977). Also in re Al-GaAs, see J. R. Chelikowsky, S. G. Louie and M. L. Cohen, *Solid State Commun.* **20**, 641 (1976).
- ²¹J. Harris and G. S. Painter, *Phys. Rev. Lett.* **36**, 151 (1976); R. P. Messmer, C. W. Tucker, Jr., and K. H. Johnson, *Surf. Sci.* **42**, 341 (1974); I. P. Batra and P. S. Bagus, *Solid State Commun.* **16**, 1097 (1975); I. P. Batra and O. Robaux, *Surf. Sci.* **49**, 653 (1975); N. Rösch and D. Menzel, *Chem. Phys.* **13**, 243 (1976); C. H. Li and J. W. D. Connolly, *Surf. Sci.* **65**, 700 (1977); R. P. Messmer and D. R. Salahub, *Phys. Rev. B* **16**, 3415 (1977). Cf. also A. van der Avoird, H. de Graaf, and R. Berns, *Chem. Phys. Lett.* **48**, 407 (1977).
- ²²T. B. Grimley and E. E. Mola, *J. Phys. C* **9**, 3437 (1976).
- ²³Refs. 14 and 15 summarize certain aspects of this work. Compare J. R. Smith, S. C. Ying, and W. Kohn, *Phys. Rev. Lett.* **30**, 610 (1973); *Phys. Rev. B* **11**, 1483 (1975); H. B. Huntington, L. A. Turk, and W. W. White III, *Surf. Sci.* **48**, 187 (1975); L. M. Kahn and S. C. Ying, *Solid State Commun.* **16**, 799 (1975).
- ²⁴J. R. Smith, *Phys. Rev.* **181**, 522 (1969).
- ²⁵N. D. Lang and W. Kohn, *Phys. Rev. B* **1**, 4555 (1970); **3**, 1215 (1971).
- ²⁶Cf. also A. J. Bennett and C. B. Duke, in *Structure and Chemistry of Solid Surfaces*, edited by G. A. Somorjai (Wiley, New York, 1969).
- ²⁷Cf. T. B. Grimley, *Proc. Phys. Soc.* **90**, 751 (1967); D. M. News, *Phys. Rev.* **178**, 1123 (1969); J. W. Gadzuk, in *Structure and Chemistry of Solid Surfaces*, edited by G. A. Somorjai (Wiley, New York, 1969); A. van der Avoird, *Surf. Sci.* **18**, 159 (1969); H. Suhl, J. H. Smith, and P. Kumar, *Phys. Rev. Lett.* **25**, 1442 (1970); J. R. Schrieffer and R. Gomer, *Surf. Sci.* **25**, 315 (1971); R. H. Paulson and J. R. Schrieffer, *Surf. Sci.* **48**, 329 (1975); S. K. Lyo and R. Gomer, *Phys. Rev. B* **10**, 4161 (1974); W. Brenig and K. Schönhammer, *Z. Phys.* **267**, 201 (1974); A. Madhukar and

- B. Bell, *Phys. Rev. Lett.* **34**, 1631 (1975); A. Bagchi and M. H. Cohen, *Phys. Rev. B* **9**, 4103 (1974); **13**, 5351 (1976).
- ²⁸The authors of Ref. 18 used a spin-polarized formalism and found no spin polarization for the H atom in the region of equilibrium. (O. Gunnarsson, private communication.)
- ²⁹The parameter ν_s is defined by $\frac{4}{3}\pi r_s^3 = 1/\bar{n}$ with \bar{n} the positive background density.
- ³⁰L. Hedin and B. I. Lundqvist, *J. Phys. C* **4**, 2064 (1971).
- ³¹P. Roman, *Advanced Quantum Theory* (Addison-Wesley, Reading, Mass., 1965), p. 298.
- ³²A. R. Williams and J. van W. Morgan, *J. Phys. C* **7**, 37 (1974).
- ³³Note that we do not use an l expansion to compute the unscattered wave here; it is obtained directly as in Ref. 25.
- ³⁴Only values of E below the vacuum level are of interest to us here. Our use of both regular and irregular solutions in Eq. (2.21) allows us to avoid a spectral representation of the Green's function, i.e., one which requires solutions of all energies, including those which propagate in the vacuum.
- ³⁵We omit writing a degeneracy index, because it is never needed in practice.
- ³⁶ $\Theta(x) = 1$ for $x > 0$, and $\Theta(x) = 0$ for $x < 0$.
- ³⁷The input $\delta n(\vec{r})$ to each iteration was taken to be a mixture of the input and the output $\delta n(\vec{r})$ of the previous iteration. The initial (trial) $\delta n(\vec{r})$ was usually the free-atom density, although sometimes it was just taken to be a one-parameter exponential function.
- ³⁸It was generally found sufficient in the calculations presented in Sec. III to take $R \sim 6$ bohrs.
- ³⁹Free-atom properties were calculated using a spin-polarized local-density program written by J. F. Janak (private communication). The free-atom electron density was made spherically symmetric by partially filling the discrete atom levels where necessary. (For H, the exact total energy of -1 Ry was used to calculate ΔE_d .)
- ⁴⁰J. B. Pendry, *J. Phys. C* **10**, 809 (1977).
- ⁴¹A. R. Williams and N. D. Lang, *Phys. Rev. Lett.* **40**, 954 (1978).
- ⁴²R. F. W. Bader, W. H. Henneker, and P. E. Cade, *J. Chem. Phys.* **46**, 3341 (1967); R. F. W. Bader, I. Keaveny, and P. E. Cade, *J. Chem. Phys.* **47**, 3381 (1967).
- ⁴³This behavior was also studied in Ref. 19, and discussed using an analytic model by J. P. Muscat and D. M. Newns, *Phys. Lett. A* **61**, 481 (1977); **60**, 348 (1977).
- ⁴⁴When the atom is moved deep inside the metal (for the $\nu_s = 2$ case shown here), the resonance drops down to a position just below the band edge, becoming a discrete state, as shown by C. O. Almbladh, U. von Barth, Z. D. Popovic, and M. J. Stott, *Phys. Rev. B* **14**, 2250 (1976). Cf. also E. Zaremba, L. M. Sander, H. B. Shore and J. H. Rose, *J. Phys. F* **7**, 1763 (1977).
- ⁴⁵In the jellium model, this change of sign occurs at the positive background edge.
- ⁴⁶Such a splitting has been observed by S. A. Flodström, C. W. B. Martinsson, R. Z. Bachrach, S. B. M. Hagström, and R. S. Bauer [*Phys. Rev. Lett.* **40**, 907 (1978)] for oxygen adsorption on Al(111). It is not observed in experiments on polycrystalline Al in which the oxygen penetrates the surface [K. Y. Yu, J. N. Miller, P. Chye, W. E. Spicer, N. D. Lang, and A. R. Williams, *Phys. Rev. B* **14**, 1446 (1976)]. The latter paper also shows that reintroduction of the discrete substrate lattice (as in Appendix D) leads to a metal-atom separation for which the lower panel of Fig. 8 would be appropriate. See also the paper of W. Eberhardt and C. Kunz (unpublished) for the adsorption of oxygen on Al(100) and Al(110).
- ⁴⁷Compare e.g., B. I. Bennett and A. A. Maradudin, *Phys. Rev. B* **5**, 4146 (1972).
- ⁴⁸R. L. Matcha and S. C. King, Jr., *J. Am. Chem. Soc.* **98**, 3415 (1976); **98**, 3420 (1976).
- ⁴⁹Compare also G. C. Lie, *J. Chem. Phys.* **60**, 2991 (1974).
- ⁵⁰Such effects are also discussed in Ref. 19.
- ⁵¹J. C. Slater, *The Self-Consistent Field for Molecules and Solids: Quantum Theory of Molecules and Solids* (McGraw-Hill, New York, 1974), Vol. 4.
- ⁵²Some of this evidence is cited in footnote 7 of K. Y. Yu *et al.*, Ref. 46.
- ⁵³The distance d is held constant, since we imagine the electron to be removed in an x-ray photoemission experiment (Franck-Condon principle).
- ⁵⁴A. Messiah, *Quantum Mechanics* (North-Holland, Amsterdam, 1961), Vol. I, p. 489.
- ⁵⁵The integration over azimuthal angle ϕ can be done trivially here because of the cylindrical symmetry; we retain a complete integral over solid angle only for convenience of notation.
- ⁵⁶In the numerical solution of these equations, components l' of the product of Ψ_{Eml} and the potential are taken to be zero when $l' > l + 2$ and $r < 0.2$ bohr. This eliminates a potential instability in our numerical procedure. [Small errors in $C_{Emll'}(r)$, the coefficient of $j_{l'}(pr)$, introduced at small radii are amplified at large radii by the enormous increase in $j_{l'}(pr)$ for large l' .]
- ⁵⁷It is more convenient for numerical reasons to evaluate this coefficient, insofar as it is explicitly used in the equations of Sec. II, according to the procedure described in the text; and to evaluate it, insofar as it appears in G_{Eml}^M using the procedure described in Appendix B.
- ⁵⁸Since we use this series in evaluating Eq. (B2), we are assuming that there are no singularities in the bare-metal potential in the vicinity of the origin. In the special case in which the adatom nucleus is at the positive background edge, however, this is not true, because the second derivative of this potential is discontinuous there, which implies a discontinuity in the fourth derivative of the wave function. This circumstance is of little importance, and we take no account of it in this analysis.
- ⁵⁹G. N. Watson, *A Treatise on the Theory of Bessel Functions*, 2nd ed. (Cambridge U. P., Cambridge, 1952), p. 379.
- ⁶⁰U. W. Hochstrasser, in *Handbook of Mathematical Functions*, edited by M. Abramowitz and I. A. Stegun (Nat. Bureau of Standards, Washington, D.C., 1965), Sec. 22 [22.3.4 and 22.5.37].
- ⁶¹Over most of this range, u_{Ek}^M and \bar{u}_{Ek}^M have an exponential rather than oscillatory character in the metal. Over the range in which the exponential decay length is very short (large κ), it is convenient to extract an

exponential from these wave functions and numerically integrate only the differential equation for the remaining factor.

⁶²The potential due to the charges outside the sphere is included when solving Eq. (A2) (and the corresponding equation for S), but we continue to truncate the integral in Eq. (2.1) at the sphere boundary, implying in particular that we use Eq. (2.24) in the form it is given to evaluate the coefficients α_{Emk}^{MA} , because the fractional error introduced thereby into, e.g., the dipole moment can be shown to be $O((2k_F R)^{-3})$.

⁶³We give some examples illustrating this point for Si and Na chemisorbed at their equilibrium distances on a high-density ($r_s = 2$) substrate. (Sphere radius $R = 6$ bohrs.) For Na, when the charges outside the sphere are fully taken into account, the dipole moment $\mu = 3.2$ D; when no account is taken of these charges, $\mu = 2.7$ D. (If only the direct effect is included, $\mu = 3.4$ D, which exemplifies cancellation between direct and indirect effects.) For Si, when the charges outside are fully taken into account, $\mu = -0.9$ D; when no account is taken of these charges, $\mu = -1.1$ D. (If only the direct effect is included, $\mu = -0.7$ D.) When R is increased from 6 to 7 bohrs (an increase of $\sim \frac{1}{3}$ Friedel wavelength), the computed value of μ when the charges outside are fully taken into account is stable to 0.05 D (Si).

⁶⁴Although this charge distribution decreases monotonically with distance along the surface, there is in fact also an oscillatory distribution that is confined to the surface, as discussed by T. B. Grimley, Proc. Phys. Soc. **92**, 776 (1967). The amplitude of this distribution decreases much more rapidly with distance however ($\sim R^{-5}$), and so we take no account of it here. See also T. L. Einstein, Crit. Rev. Solid State Sci. (to be published).

⁶⁵A similar result has been given by T. B. Grimley (Ref. 64) and by J. Rudnick [Phys. Rev. B **5**, 2863 (1972)]. See also D. E. Beck, V. Celli, G. Lo Vecchio, and A. Magnaterra, Nuovo Cimento B **68**, 230 (1970). The analysis indicates that $\delta n(\vec{r}, E) \sim \xi B(\xi, \theta) r^{-2} \sin^2 \xi^{1/2} \times [2r + \beta(\xi, \theta)]$ for large r , and $r \cos \theta$ in the region where Eq. (2.15) is valid, with $\xi \equiv E - E_0$ (E_0 is the bottom of the metal band) and B and $\beta \rightarrow$ constants (which can be θ dependent) as $\xi \rightarrow 0$. Integration of this over ξ from 0 to $E_F - E_0$ gives Eq. (C1) to leading order in $(2k_F r)^{-1}$. Integration over \vec{r} outside the sphere gives a correction to that state density change $\delta n(E)$ which would be calculated from Eq. (2.29) by integrating only over the sphere. The parameters in this correction can be obtained by fitting to computed results at the sphere surface, just as in the case of Eq. (C1). This correction, it is found, would generally not be visible in graphs of $\delta n(E)$ of the type presented in this paper, except in the case of hydrogen (Fig. 5). Failure to include this correction in that figure would have led to the presence of a small additional hump in the curve. (This is seen in Fig. 2 of Ref. 14, which does not include it, and remnants of such humps are seen in Fig. 2 of Ref. 19.) Note, however, that we have not included in the figure any contribution to $\delta n(E)$ associated directly with the dipole-induced surface charge outside the sphere, since we expect this contribution to be rather structureless

(and small).

⁶⁶ z_F can be taken to be the position of the positive-background edge.

⁶⁷Choosing R so as to make μ_F zero is not convenient, since this value of R could change as the iteration proceeds, and it certainly changes when the adatom is changed, whereas we want to evaluate the bare-metal Green's function [as it appears in Eq. (2.24)] only once for a given R (and d), and not have to evaluate it again. Furthermore, an R value which corresponds to a zero dipole-moment correction might correspond to the maximum value in the correction to some other quantity.

⁶⁸N. D. Lang and W. Kohn, Phys. Rev. B **7**, 3541 (1973).

⁶⁹Rudnick (Ref. 65) discusses a charge distribution of this type also.

⁷⁰We obtain a perturbative correction to the atomic binding energy due to the small amount of charge outside the sphere by making the local-density approximation to the total nonelectrostatic energy density in the region outside the sphere. This approximation, together with Eq. (3.1) of Ref. 9, gives the result shown.

⁷¹We neglect changes from the bulk value in the lattice spacing at the surface (and other possible distortions) both in the case of the bare metal and in the case of the metal-adatom system, because such changes are generally found to be small for the closest-packed crystal faces, to which our discussion is most applicable. For Al(111), for example, the spacing of the outermost two lattice planes in the case of the clean surface is found to differ from its bulk value by $\sim 3\%$ [D. W. Jepsen, P. M. Marcus, and F. Jona, Phys. Rev. B **6**, 3684 (1972) and **8**, 1786E (1973).]

⁷²Cf., e.g., J. K. Grepstad, P. O. Gartland, and B. J. Slagsvold, Surf. Sci. **57**, 348 (1976).

⁷³J. P. Perdew and R. Monnier, Phys. Rev. Lett. **37**, 1286 (1976).

⁷⁴N. W. Ashcroft, Phys. Lett. **23**, 48 (1966); N. W. Ashcroft and D. C. Langreth, Phys. Rev. **155**, 682 (1967).

⁷⁵The pseudopotential cores do not overlap.

⁷⁶Atom-jellium model results for $r_s = 2$ were used.

⁷⁷The centered adsorption site over an atom in the second layer is found to give a binding energy $\sim \frac{1}{2}$ eV smaller than that for the centered site over a hole in the second layer.

⁷⁸This is also the usual experimental result. See, e.g., F. Forstmann, W. Berndt, and P. Büttner, Phys. Rev. Lett. **30**, 17 (1973) [In re I-Ag(111)]; J. E. Demuth, D. W. Jepsen, and P. M. Marcus, Phys. Rev. Lett. **32**, 1182 (1974) [In re S-Ni(111)].

⁷⁹P. M. Marcus, J. E. Demuth, and D. W. Jepsen, Surf. Sci. **53**, 501 (1975). See also the discussion of Si-Mo(001) by A. Ignatiev, F. Jona, D. W. Jepsen, and P. M. Marcus, J. Vac. Sci. Technol. **12**, 226 (1975).

⁸⁰The metallic radius is half the nearest-neighbor distance in the bulk metal.

⁸¹We use the value for the covalent radius given by L. Pauling in *The Chemical Bond* (Cornell University, Ithaca, 1967), p. 136.

⁸²A similar result is found for H-Al(111) in Ref. 18.

⁸³See also the discussion of the adsorption of oxygen on aluminum in K. Y. Yu *et al.*, Ref. 46.